Desalination and Water Treatment
www.deswater.com

doi: 10.5004/dwt.2018.21968

112 (2018) 119–146
April

A comparative study on phyllosilicate and tectosilicate mineral structural properties

Marinos Stylianou[a], Vassilis Inglezakis[b,*], Agapios Agapiou[c], Grigorios Itskos[d], Albina Jetybayeva[b], Maria Loizidou[e]

[a]*University of Cyprus, Department of Civil and Environmental Engineering, NIREAS-International Water Research Center, Subsurface Research Laboratory, Nicosia, Cyprus*
[b]*Nazarbayev University, School of Engineering, Chemical Engineering Department, Astana, Kazakhstan, email: vasileios.inglezakis@nu.edu.kz (V. Inglezakis)*
[c]*University of Cyprus, Department of Chemistry, P.O. Box 20537, 1678 Nicosia, Cyprus*
[d]*Purdue University, School of Materials Engineering, West Lafayette, IN 47907, USA*
[e]*National Technical University of Athens, School of Chemical Engineering, Unit of Environmental Science and Technology (UEST), Athens, Greece*

Received 16 October 2017; Accepted 25 January 2018

ABSTRACT

Natural minerals are widely used in numerous environmental applications, mainly as sorbents in ion exchange and sorption processes. Minerals, such as zeolites and clays, can be found all over the world, but they are mined containing a variety of different impurities; this prevents their accurate characterization. The present study examines various methods used for the characterization of three common natural silicate minerals, one zeolite (clinoptilolite) and two clays (montmorillonite and vermiculite). Their characterization was performed through a series of analytical measurements so as to gather all the information needed regarding their structural properties. Therefore, "similar" minerals such as clinoptilolite vs. heulandite and vermiculite vs. hydrobiotite can be distinguished; revealing important properties when comes to their practical application. The methods used in the present study are X-ray powder diffraction (XRD), X-ray fluorescence, Fourier transform infrared (FTIR) spectroscopy, TG/DTG/DTA and N_2-porosimetry (BET). An extensive literature review of the natural silicate minerals has been conducted and the relevant results and methods are comparatively reported. The analytical results enabled the distinguish of the examined minerals. XRD, FTIR, TG/DTG/DTA showed that all three minerals have characteristic bands that can be used to easily distinguish from others.

Keywords: Bentonite; Brunauer–Emmett–Teller; Characterization; FTIR; Ion exchange; TG/DTA; Vermiculite; XRD; XRF, Zeolites

1. Introduction

Zeolites and clays are considered suitable materials for a wide variety of industrial and environmental applications as liquid and gas phase adsorption tools. This is due to their worldwide abundance, their low cost, their high cation exchange capacity (CEC) and their porous structure [1–3].

Clinoptilolite is one of the most abundant natural zeolites. Its structure is generally described as an outer tetrahedral framework of silica and alumina, within which migration of water molecules and exchangeable cations (Ca^{2+}, K^+ and Na^+) may occur [4,5]. Bentonite rock main component is montmorillonite mineral which consists of clay layers that form lamellar platelets, held

* Corresponding author.

Presented at the 5th International Conference on Sustainable Solid Waste Management (ATHENS 2017), 21–24 June 2017, Athens, Greece.

together by electrochemical forces. Each platelet is formed by three arranged layers: two tetrahedral silica (SiO_2) layers around a central octahedral alumina (Al_2O_3) layer [6]. Vermiculite is typical clay which belongs to the montmorillonite–vermiculite group. The general structure of vermiculite can be described as a silicate sheet consisted of two flat layers of silica and alumina tetrahedral layers joined in an octahedral layer of oxygen, magnesium, iron atoms and hydroxyl molecules [7]. An extended literature review on the environmental applications of these materials is summarized in Table 1.

A variety of analytical instruments are used for the structural, physical and chemical characterization of natural minerals. Among others, the most popular are: Fourier transform infrared spectroscopy (FTIR), X-ray fluorescence (XRF), X-ray powder diffraction (XRD), thermogravimetric analysis (TGA), differential thermal analysis (DTA) and N_2-porosimetry. In the present study, each analytical technique is presented and discussed in detail. Literature data are compared in relation to the analytical results obtained from the different minerals.

FTIR produces an infrared absorption spectrum to identify chemical bonds and to detect functional groups in a molecule. In total, 29 samples are collected and discussed; 15 for clinoptilolite, 8 for bentonite and 6 for vermiculite. XRF is applied to determine the chemical composition of minerals, including Si/Al ratio, which is an important parameter for these minerals. Thus, data of 39 samples are collected; 21 for clinoptilolite, 12 for bentonite and 6 for vermiculite. XRD is a rapid analytical technique primarily used for phase identification of crystalline materials. Therefore, 27 samples are collected and analyzed; 13 for clinoptilolite, 4 for bentonite and 10 for vermiculite. TGA is a thermal analysis method in which changes in physical and chemical properties of materials are measured as a function of temperature. TG/DTG/DTA analysis is very important when characterizing natural minerals because of the information that can be collected for their nature and chemical species that can be lost upon heating. Also, important parameters can be obtained from endothermic and exothermic peaks present on DTA curves, showing the dehydration and amorphization/recrystallization of a mineral [8]. In total, 48 samples are presented; 25 for clinoptilolite, 12 for bentonite and 11 for vermiculite. Finally, Brunauer–Emmett–Teller (BET) analysis provides information on the surface area, pore volume and pore size distribution of materials. In total, 19 samples are included and discussed; 10 for clinoptilolite, 5 for bentonite and 4 for vermiculite.

In the present study, the importance of three different natural minerals (clinoptilolite, bentonite, vermiculite), widely employed in sorption technologies is highlighted. Their analytical characterization is performed using a number of analytical techniques. The experimental findings are presented, commented and widely discussed and compared with literature. According to our knowledge, very few studies present such a complete data set. This information can be used by environmental scientists, which focus on the study of natural silicate minerals in environmental applications. The present study provides all the necessary steps so as to distinguish the minerals under study between others, with similar characteristics.

2. Materials and methods

2.1. Examined silicate minerals

Three different natural minerals were used in this study: zeolite (clinoptilolite, <5 mm), vermiculite (<5 mm) and bentonite (<90 μm). Zeolite and bentonite were supplied by S&B Industrial Minerals SA (Greece) and vermiculite by IGME (Institute of Geology & Mineral Exploration, Greece). Clinoptilolite and vermiculite were further crushed and milled into powder (<90 μm), prior to further analysis.

2.2. Mineral characterization methods

2.2.1. FTIR spectroscopy

An FTIR spectrophotometer (Perkin Elmer 880 spectrometer) was used to measure the infrared absorption on the three mineral samples. The FTIR spectra in the 4,000–400 cm^{-1} range were recorded for all minerals at room temperature. Samples were prepared by the standard KBr pellets method. Solid samples have been milled together with potassium bromide (KBr) to form a very fine powder, which is then uniaxially compressed into a thin pellet that can be further analyzed.

2.2.2. X-ray fluorescence

The samples were ground (<90 μm) to eliminate large and/or inconsistent grain sizes and then compressed into pellets to be subjected to XRF analysis, by means of an ARL Advant XP sequential (wavelength dispersive) system. It is noted that prior to being compressed, vermiculite samples were dried at 105°C and kept in a desiccator, as this mineral is particularly hydroscopic and its powders may damage the compression dies by sticking to their metallic walls.

2.2.3. X-ray diffraction

The powder X-ray diffraction patterns of the mineral samples were recorded on a Siemens D-5000 X-ray powder diffractometer over 2θ range of 5° to 55° at a scanning speed of 2° (2θ) per minute and a step size of 0.05°. The diffractometer was equipped with Ni-filtered Cu Kα radiation source (8,978 eV or λ = 1.5418 Å). The X-ray source was operated at 30 mA and 40 kV. Sample preparation for the X-ray analysis involved gentle grinding of the solid into a fine powder and packing of approximately 0.3–0.5 g of the sample into an aluminum sample holder with light compression to make it flat and tight.

2.2.4. TG/DTG/DTA thermal analysis

DTA and TGA or DTG were obtained simultaneously, by means of a Mettler Toledo 851 thermal analyzer at a heating rate of 10°C/min, using air atmosphere. The samples (10 mg) were heated in a platinum crucible in the temperature range 25°C–1,200°C. Table 2 summarizes the experimental conditions usually reported in the thermal analysis of minerals, particularly zeolite, bentonite and vermiculite, as obtained by an integrated relative literature review.

Table 1
Environmental applications of clinoptilolite, bentonite and vermiculite

No.	Mineral	Environmental application	Reference
B1	Bentonite	Remediation of acid mine drainage	[9]
B2		Attenuation of heavy metals from acidic wastewaters (Co^{2+}, Cu^{2+}, Ni^{2+}, Pb^{2+} and Zn^{2+})	[10]
B3		Removal of heavy metals from aqueous solutions	[11–15]
B4		Extractability of heavy metals from sewage sludge	[16]
B5		Copper removal from sludge permeate with ultrafiltration membranes	[17]
B6		Adsorption of polymers [poly(vinyl alcohol)] from aqueous solution	[18]
B7		Adsorption of herbicide (diuron)	[19]
B8		Immobilization and recovery of uranium(VI) from radionuclide polluted wastewater	[20]
B9		Stabilization and remediation of cadmium (Cd) and lead (Pb) co-contaminated paddy soils	[21]
B10		Pharmaceutical uses	[22]
B11		Cesium ion sorption from aqueous solution (nuclear waste)	[23]
B12		Adsorption of mercury from wastewater	[24]
B13		Use as drilling mud	[25]
B14		Ammonia removal	[26]
B15		H_2S removal	[27,28]
B16		Trapping of volatile organic sulfur derivatives	[29]
B17		Removal of CO_2	[30]
B18		Hydrogen storage	[31–33]
B19		Mercury removal from the flue gas	[34–36]
V1	Vermiculite	Removal of heavy metals from aqueous solutions	[37–50]
V2		Copper removal from sludge permeate with ultrafiltration membranes	[17]
V3		Removal of chromium from tannery effluent	[49]
V4		Cesium ion sorption from aqueous solution (nuclear waste)	[51]
V5		As catalyst for the Fenton reaction	[52]
V6		Adsorption of phthalates	[53]
V7		Ammonia removal	[26]
V8		Air purification (volatile organic compounds removal)	[54]
V9		Desulfurization of exhaust gases	[55]
C1	Clinoptilolite	Removal of heavy metals from aqueous solutions	[15,37,56–78]
C2		Removal of ammonia	[67,79–85]
C3		Adsorption of aflatoxin	[86]
C4		Additive in composting process	[87]
C5		Additive in sewage sludge composting process	[88]
C6		Purification of metal electroplating waste waters	[89]
C7		Animal dietary addition; animal health	[90–102]
C8		As active carrier for antibiotics in antiacne topical therapy	[103]
C9		Medical and biomedical applications	[104,105]
C10		Stabilization of metal contaminated soils	[106–108]
C11		Cesium ion sorption from aqueous solution (nuclear waste)	[109]
C12		As amendments in radiocaesium and radiostrontium contaminated soils	[110]
C13		Additive in composting process	[108,111–113]
C14		Immobilization of selected heavy metals in sewage sludge	[114]
C15		The effect on the serotonergic receptors in the brain of mice with mammary carcinoma	[115]
C16		Uses in agriculture and industry	[116]
C17		Medical applications; adjuvant in anticancer therapy	[117–120]
C18		Uptake and release of phosphorus	[121]
C19		Removal of H_2S	[122]
C20		Natural gas upgrading (removal of N_2, NH_3)	[123–125]

(continued)

Table 1 *(continued)*

No.	Mineral	Environmental application	Reference
C21		Natural gas purification (removal of CO_2)	[126]
C22		Ar enrichment (removal of O_2)	[127]
C23		Air prepurification (removal of CO_2)	[127]
C24		Exhaust gas cleanup (removal of NO_x)	[128]

Table 2
Conditions used for the thermal analysis of minerals under study

Reference	Temperature (°C)	Heating rate	Gas atmosphere	Crucibles	Reference standard
Zeolite					
[129]	20–1,000	10°C/min	Air	Platinum	Al_2O_3
[130]	20–750	10°C/min	Static air	–	–
[131]	20–1,200	10°C/min	Static air	–	–
[132]	30–1,000	10°C/min		–	–
[133]	20–1,200	10°C/min	Air	–	–
[134]	20–700	5°C/min	Air	–	–
[135]	25–1,000	10°C/min	Air (100 mL/min)	Platinum	–
[136]	25–1,025	10°C/min	Air	Platinum	–
[137]	25–1,100	10°C/min	Static air	–	Al_2O_3
[138]	25–900	9°C/min		–	Al_2O_3
[139]	25–1,050	10°C/min	N_2	Platinum	α-Alumina
Bentonite					
[140]	20–1,200	10 K/min	N_2	–	α-Al_2O_3
[141]	25–1,000	10°C/min	N_2	–	α-Alumina
[142]	20–800	10°C/min	N_2 (120 mL/min)	–	–
[143]	20–1,000	10°C/min	N_2	–	Calcinated α-alumina
[144]	20–1,000	10°C/min	N_2 (80 mL/min)	–	Calcinated α-alumina
[145]	25–1,100	10 K/min	N_2	–	α-Al_2O_3
Vermiculite					
[146]	25–1,000	5°C/min and 15°C/min	Air	Platinum	Calcined alumina
[147]	25–1,100	6 K/min	Air (40 mL/min)	Corundum	–
[148]	25–1,020	10°C/min	–	–	–
[149]	25–1,000	12°C/min	Air	–	–
[150]	25–1,000	10 K/min	Air	–	–
[151,152]	20–1,200	10 K/min	Air	–	–

2.2.5. Capacity measurements

In general, seven types of capacities can be defined [153,154]: ideal exchange capacity, theoretical exchange capacity (TEC), real exchange capacity, maximum exchange level (MEL), operating capacity, breakthrough capacity and effective capacity. "Ideal exchange capacity" corresponds to the actual amount of exchangeable cations and is a characteristic property of pure zeolite species. In nature, zeolites exist not in pure forms but as zeolite tuffs, containing several impurities. These impurities play an important role to the value of ion-exchange capacity. In relation to their activity (active or inactive in respect to ion exchange) they can increase or decrease capacity. The amount of possible exchangeable cations of a zeolite sample (tuff) with a specific purity is expressed with TEC. TEC is an overestimation of the exchange ability of the material due to the fact that some of the zeolite tuff cations are part of impurities or they are not available for ion exchange. Thus, real exchange capacity is introduced, which is defined as the amount of all removable cations and is equal to the active negative charge of the zeolite framework.

Effective capacity (EC) is defined as the amount of cations of the zeolite contained in a specific amount of the material, which are exchangeable under specific experimental conditions. EC is equal to MEL when an infinite contact time and ratio of solution to volume of solid mass are utilized. The operating capacity is used in fixed bed ion-exchange models, as it is expressing the part of MEL that is available in the specific column operation. Breakthrough capacity is the capacity utilized in column operations and is used for the determination of selectivity series and for the design of column operations.

Most commonly used in the characterization of minerals are the TEC and the MEL. A common method for the

determination of the TEC of ion exchangers is the chemical analysis. For natural minerals containing impurities, which can be active or inactive with respect to ion exchange, TEC is expressing the amount of potential exchangeable cations. The most common exchangeable cations are Mg, Ca, K and Na. Thus, TEC is the total sum of the mineral exchangeable cations. MEL is a characteristic property of the specific ion-exchange system. An ion-exchange system is defined as a system consisting of a material and a liquid solution which contains the ion to be exchanged, under a specified temperature and normality. MEL is straightforwardly related to the equilibrium behavior of the specific ion-exchange system and like the equilibrium isotherm depends only on the temperature and the normality of the solution. MEL is measured by repeated equilibrations or by determinations using equilibrium data (equilibrium isotherm) and is expressed in terms of exchangeable ions per unit mass of the exchange material [153]. In the present study, MEL experiments were conducted as follows: a measured quantity of zeolite, bentonite or vermiculite (0.2–0.8 g) was added in a vessel containing specific volume of metal solutions (100 cm^3) at the initial concentration of 0.01 N, with pH initial adjustment (pH = 4). Every 7 d the solution was analyzed for metal concentrations and then replaced with fresh solution of the same metal, until no further uptake from mineral was observed.

2.2.6. Specific surface area and porosity

The most widely used technique for estimating surface area is the so-called BET method [155]. BET is a well-known equilibrium model for the physical adsorption of gas molecules on a solid surface and is the basis for the measurement of the specific surface area (SSA) of a material [155,156]. The SSA and the pore characteristics of minerals (50 mg) were determined volumetrically by physisorption of N_2 at normal boiling point temperature (77 K) in a static mode using a Nova-2000 6.11 Quantachrome instrument. The pretreatment (degassing) of the samples took place under vacuum (10^{-2} Torr) at 150°C.

3. Results and discussion

3.1. FTIR spectroscopy

Natural minerals, such as zeolites, montmorillonites and vermiculites, are used in ion-exchange systems because of some specific characteristics regarding their structure, channel size and cation substitution in the tetrahedral sites of the minerals, which makes them proper materials for such systems. FTIR spectroscopy is powerful tool for the determination of the chemical composition and identification of the functional groups of minerals [133].

In general, FTIR spectra of zeolites are characterized by bands occur at different regions of cm^{-1} [133]:

1. The region of 3,700–1,600 cm^{-1}: bands are attributed to zeolite water [136,157]. In this region, three typical bands are observed [133]:
   a) Close to ~3,620 cm^{-1}: OH stretching vibration.
   b) Close to ~3,440 cm^{-1}: the band that is characteristic of hydrogen bonding of the water to surface oxygen ions.
   c) Close to ~1,630–1,640 cm^{-1}: OH bending vibration of water.
2. Regions 1,200–950 and 420–500 cm^{-1}: bands due to Si–O–Si and Si–O–Al vibrations.
   a) In the region 1,200–650 cm^{-1} strong vibration bands appear which are attributed to the internal tetrahedron vibrations, and are assigned to symmetric (~670 cm^{-1}) and asymmetric (~1,030–1,060 cm^{-1}) T–O stretching mode.
   b) In the second region 420–500 cm^{-1}, the band is attributed to T–O bending mode (where T is SiO4 or AlO4) [133,136,157,158].
3. The region of 500–800 cm^{-1}: bands due to pseudo-lattice vibrations, which are insensitive to the nature of the channel cations, and to the Si/Al ratio [133,136,157].

The basic findings by the FTIR spectroscopy characterization of the examined zeolite samples are summarized below:

1. Bands attributed to zeolite water in the region of 3,700–1,600 cm^{-1}:
   a) OH-stretching: the band of zeolite under study is found at ~3,622 cm^{-1}, which is attributed to the interactions of the water hydroxyl with the cations. Bands in Table 3 show very close bands for clinoptilolite and heulandite, with values close to 3,620 cm^{-1}.
   b) Hydrogen bonding of the water to surface oxygen: the band of zeolite under study is found at ~3,446 cm^{-1}. From Table 3, it can be seen that the bands for clinoptilolite and heulandite are very close, with values in the range of 3,413–3,459 cm^{-1} for clinoptilolite, 3,420 cm^{-1} for heulandite and 3,437–3,450 cm^{-1} for heulandite type-II.
   c) OH-bending: bending mode of the water is found at ~1,635 cm^{-1} [133]. Table 3 reports literature data concerning this band group. Clinoptilolite bands are from 1,630 to 1,650 cm^{-1}, heulandite bands are in the same range, while heulandite values close to 1,638–1,640 cm^{-1}.
2. Bands attributed to the Si–O–Si and Si–O–Al vibrations in the regions 1,200–950 and 420–500 cm^{-1}:
   a) Asymmetric T–O stretching: the strongest T–O stretching vibration appears at 1,036 cm^{-1}, which as reported by Perraki and Orfanoudaki [133], is a very significant band for the estimation of aluminum content in the crystalline framework and it depends on the Al/Si ratio. It shifts to a lower wave number with increasing number of Al atoms in the framework tetrahedral sites [133]. In general, clinoptilolites have less Al atoms per formula unit in relation to heulandites, and TO-stretching band is expected to be found in higher wavelength values than in heulandites. Mozgawa et al. [157] compared a clinoptilolite with six Al atoms per formula unit with a heulandite with nine Al atoms per formula unit, and reported a clinoptilolite peak at 1,059 cm^{-1}, while heulandite showed a peak at 1,022 cm^{-1} [157]. Comparing these results with other data from Table 3, it can be seen that in general heulandites are indeed in lower wavelength values (1,022–1,030 cm^{-1}), where clinoptilolite are in higher ones but some are very close to heulandites (1,032–1,088 cm^{-1}). Perraki and Orfanoudaki [133], reported a heulandite type-II zeolite, with an intermediate content in Al atoms per formula unit, which gave a peak at 1,045 cm^{-1} [133].

Table 3
IR spectral data of clinoptilolites

Mineral	Asymmetric T–O stretching (cm^{-1})	Symmetric T–O stretching (cm^{-1})	T–O bending (cm^{-1})	OH-stretching (cm^{-1})	OH-bending (cm^{-1})	Hydrogen bonding of the water to surface oxygen (cm^{-1})	Pseudo-lattice band (cm^{-1})	Pore opening (cm^{-1})	Reference
Clinoptilolite	1,036	668	420–500	3,622	1,635	3,446	610		Present Study
Heulandite type-II	1,045	–	469	3,626	1,640	3,450	597	–	[163]
Heulandite type-II	1,045	668	420–500	3,620	1,640	3,440	597		[133]
Heulandite type-II	1,047	–	466	3,619	1,638	3,437	–	–	[160]
Heulandite	1,030	670	440	3,550; 3,640	1,650	3,420	–	420	[159]
Heulandite	1,022	658	449	–	1,642	–	594	–	[157]
Clinoptilolite	1,059	671	461	–	–	–	602	–	[157]
Heulandite (Greece)	1,034	662	464	3,600–3,620	1,630	3,420	600	514	[158]
Heulandite (Armenia)	1,028	670	466	3,600–3,620	1,630	3,420	604	521	[158]
Clinoptilolite (Georgia)	1,032	670	462	3,600–3,620	1,630	3,420	610	524	[158]
Clinoptilolite	1,088	–	480	3,640	1,650		615	–	[136]
Clinoptilolite	1,028	656	–	3,622	1,639	3,413	614	–	[129]
Clinoptilolite	1,088	–	473	3,625	1,636	3,459	606		[162]
Clinoptilolite	1,048	679	470	3,605	1,636	3,450	602	524	[135]
Mordenite[a]	1,028; 1,064	635	–	3,614	1,641	3,418	567	506	[129]

[a]Moredenite is included because its constitute of clinoptilolite ores and its peaks are close to those of clinoptilolite.

b) Symmetric T–O stretching: most bands found in literature (Table 3) are close to 670 cm^{-1}.
c) T–O bending: Table 3 reports data from the literature concerning this band group. Clinoptilolite bands are from 461 to 480 cm^{-1}, heulandite bands from 440 to 466 cm^{-1}, and heulandite type-II from 420 to 500 cm^{-1}. The intensity of the bands is autonomous to the level of crystallinity [133].

3. Pseudo-lattice vibrations: in the pseudo-lattice band range, the exact position of the vibration is found at 610 cm^{-1}. In the literature (Table 3), clinoptilolite bands are in the range of 602–615 cm^{-1}, heulandite bands 594–604 cm^{-1} and heulandite type-II at 597 cm^{-1}.

In Table 3, it can be seen that most bands of heulandites are in lower values than that of clinoptilolite [133,157]. In the study of Christidis et al. [158], for the FTIR analysis of three zeolites (two heulandites and one clinoptilolite) the bands of heulandites were in lower values than that of clinoptilolite (~10 cm^{-1}) [158]. In Table 3, it is also showed that the bands near ~520 cm^{-1} are attributed to the pore opening of the minerals [133,135,159]. From Table 3, it can be concluded that the presence of mordenite can give antisymmetrical stretching vibration of the tetrahedral T–O bonds at ~1,064 cm^{-1}, while the presence of shoulder at ~1,095 cm^{-1} is due to the presence of cristobalite and smectite with a possible contribution of amorphous silica [160,161]. Interferences may also exist by the presence of some ions and also due to the pretreatment of minerals. Korkuna et al. [129] showed that in the analysis of a Pb-containing clinoptilolite, there is an ammonia band at ~1,449 cm^{-1}, which can be connected both to absorbed ammonia complexes on palladium and to the interactions with surface acidic hydroxyl species [129]. Mozgawa [162] showed that the change of the intensity of the band at 675 cm^{-1} is linked to heavy metals sorption, and therefore this band can be considered the sorption process indicator [162].

Figs. 1 and 2 shows the FTIR spectra of bentonite as determined in the current study, while Table 4 summarizes previous relevant data reported in literature. In the

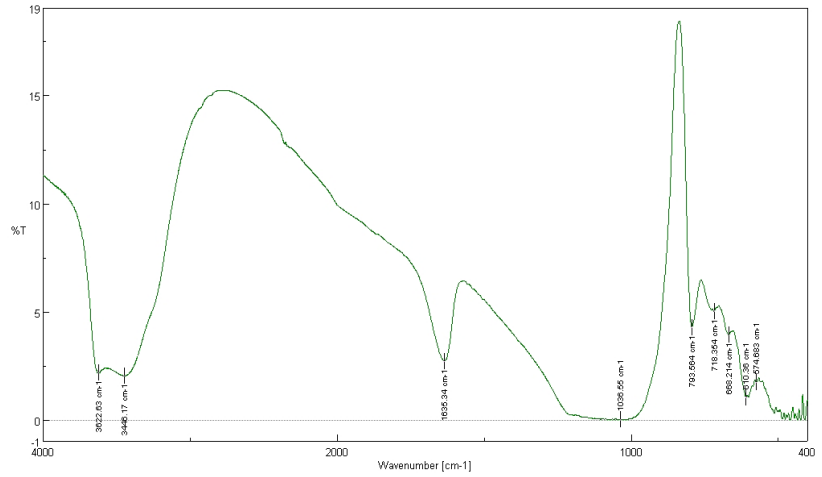

Fig. 1. FTIR spectra of clinoptilolite.

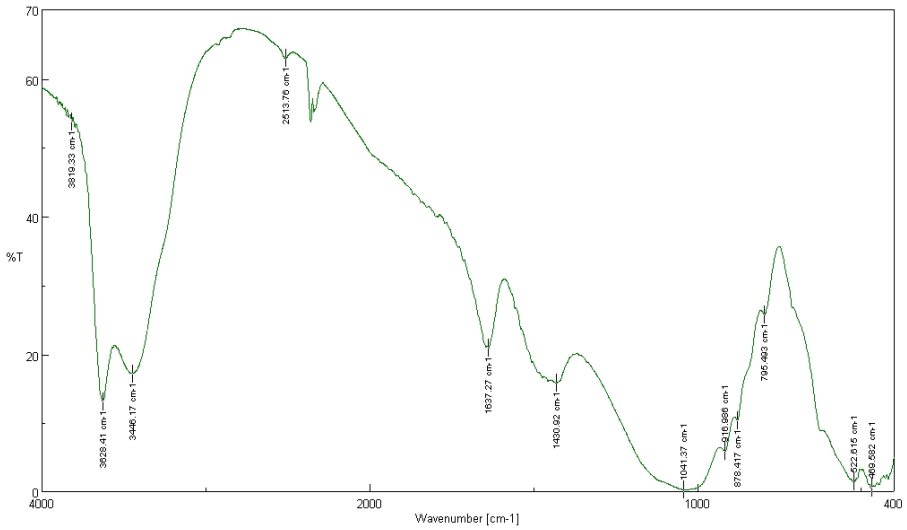

Fig. 2. FTIR spectra of bentonite.

Table 4
IR spectral data of bentonites (cm^{-1})

	Bentonite	Montmorillonite	Montmorillonite	Bentonite	Na-montmorillonite	Montmorillonite	Bentonite	Bentonite
Reference	[141,144]	[167]	[168]	[169]	[170]	[164]	[171]	Present study
Al(Mg)–O–H stretching	3,631	3,634	3,620	3,623	3,626; 3,691	3,620	3,643	3,628
H–O–H stretching (H_2O)	3,429; 3,432; 3,523	3,433	3,400	3,421	3,417	3,400	–	3,446
H–O–H bending	1,640	1,635	–	1,639; 1,643	1,643	1,640	–	1,637
CO_3 stretching of calcite and dolomite	1,430–1,382	–	–	–	–	–	–	1,430
Si–O stretching	1,115	1,115	1,100	–	–	–	1,110	–
Si–O–Si stretching	1,090; 1,045	1,040	1,040; 1,020	1,039; 1,087	1,039	–	1,045	1,047
OH bending bounded $2Al^{3+}$	919	918	915	915	–	918	920	917
OH bending bounded Fe^{3+} and Al^{3+}	888	888	–	–	–	875	881	878
OH bending bounded Mg^{2+} and Al^{3+}	843	847	–	845	–	845		
Si–O stretching of silica and quartz	798	778	–	–	–	–	797	795
Si–O stretching + in-plane bending of calcite and dolomite	710–715	671	–	–	–	–	–	
Al–Si–O bending	524	–	520	523	–	530, 516, 543	523	522
Si–O–Si bending	465	–	470	467	465	467	466	469

bentonite band, the vibrations given at 469 and 522 cm^{-1} are due to the absorption of the characteristic bond of Si–O–Si and Si–O–Al^{vi}, whereas the vibrations given at 878 and 917 and 3,628 cm^{-1}, are due to the Al^{vi}–OH–R^{vi} (where R: $A1^{3+}$, Mg^{2+}, Fe^{3+} and Fe^{2+}) [164]. Perraki and Orfanoudaki [164] reported that the vibration given at 543 cm^{-1} is characteristic of the Si–O–Al^{vi} bond and that its exact position depends on the cation that occupies the octahedral position. When substitution of Al^{vi} by Mg^{2+} takes place (Si–O–Mg^{2+} bond), a shift to lower vibration positions turns up [164,165]. The vibration given at 917 cm^{-1} refers to the Al^{vi}–OH–Al^{vi} bond and corresponds to pure montmorillonite. Smectites with high content of Mg, as a substitution of Al^{vi}(Al^{vi}–OH–Mg), vibrate at lower frequencies (845 cm^{-1}). Smectites that contain Fe, as a substitution of Al^{vi}(Al^{vi}–OH–Fe^{vi}), show vibration at ~870 cm^{-1}. In the region of 3,600–3,700 cm^{-1}, the vibration at 3,628 cm^{-1} characterizes the group of Al^{vi}–OH–Al^{vi} [164]. The low vibration at 878 cm^{-1} indicates low substitution of Al^{vi} by Fe^{3+}. Finally, the wide vibration at 3,446 cm^{-1} and the sharp vibration at 1,637 cm^{-1} are attributed to the adsorbed water.

Fig. 3 shows the FTIR spectra of vermiculite as obtained in the current study, whereas Table 5 summarizes previous relevant data reported in literature. In vermiculite band, the vibrations given at 3,419 cm^{-1} are characteristic of hydroxyl stretching vibration (OH stretch) and at 1,646 cm^{-1} they are characteristic of hydroxyl bending vibration (OH band). The vibrations at 1,013 and 457 cm^{-1} are due to Si–O stretching and Si–O–Si bending, respectively. Interferences to the IR band of clay minerals, such as montmorillonite and vermiculite, may occur due to impurities in the raw material. In the IR studies of clay, the Si–O stretching vibrations were observed at 791, 693, 539 and 469 cm^{-1}, showing the presence of quartz. The appearance of ν (Si–O–Si) and δ (Si–O) bands also support the presence of quartz. Most of the bands reported in the literature (Table 4), such as 3,697, 3,623, 3,450, 1,033, 915, 791, 693, 539 and 469 cm^{-1} are indicative of the presence of kaolinite. Furthermore, other studies in the literature report that the vibrations observed at 915 cm^{-1} indicate the possibility of the presence of hematite. Also, the presence of bands at 3,697, 3,623, 3,450, 2,370, 1,633, 1,033, 915 and 791 cm^{-1} indicate the possibility of the presence of illite, whereas 3,623, 1,633 and 1,033 cm^{-1} are indicative of gypsum and 693 cm^{-1} suggests that calcite may be present [166].

3.2. X-ray fluorescence and capacity measurements

3.2.1. X-ray fluorescence

Table 6 shows the XRF results determined in the present study, while Table 7 presents a set of relevant literature data for the three minerals under study. The overall Si/Al ratio for zeolite samples is higher than 4. As mentioned in literature, minerals with Si/Al ratio <4 are classified as heulandites, whereas Si/Al > 4 are indicative of clinoptilolites [4,174]. The SiO_2 + Al_2O_3 is higher than 75%, the rest being water and exchangeable cations. Bentonite samples show Si/Al ratio lower than 4, while SiO_2 + Al_2O_3 is higher than 65%, and in general lower than clinoptilolite samples. Finally, vermiculite samples show Si/Al ratio lower than 4, while SiO_2 + Al_2O_3

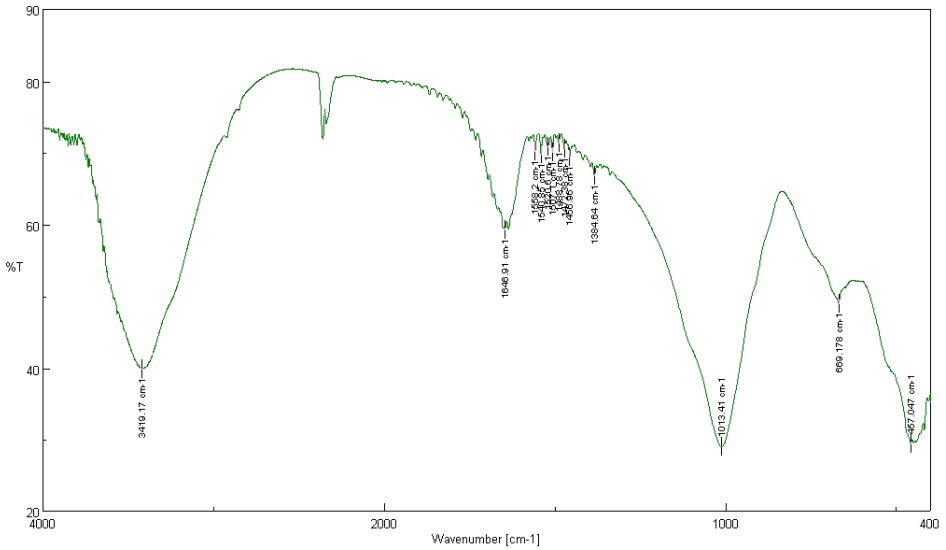

Fig. 3. FTIR spectra of vermiculite.

Table 5
IR spectral data of vermiculite

Reference	[170] (cm^{-1})	[172] (cm^{-1})	[149] (cm^{-1})	[173] (cm^{-1})	[168] (cm^{-1})	Present study (cm^{-1})
Al(Mg)–O–H stretching	3,626; 3,691	3,630	–	–	–	–
H–O–H stretching (for H_2O)	3,417	3,440	3,394	–	–	3,419
H–O–H bending	1,643	–	1,632	1,639	–	1,646
CO_3 stretching of calcite and dolomite	–	–	–	–	–	1,456
Si–O stretching	–	–	–	989	985	–
Si–O–Si stretching	1,004	–	993	1,074; 1,036	–	1,013
Si–O/Al–O vibrations	–	–	–	820	812	–
Si–O/Al–O/Al–O–Si vibrations	–	–	–	758, 726, 691, 661	670	669
Mg–O stretching	–	–	–	531, 486	–	–
Si–O–Si bending	450	–	449	461	480	457

is higher than 50%, and in general lower than clinoptilolite and bentonite samples. XRF analysis showed that vermiculite sample is rich in MgO (Mg-vermiculite) and low concentration of K_2O revealed the presence of vermiculite instead of hydrobiotite.

3.3. X-ray diffraction

3.3.1. Zeolite mineralogy

Fig. 4 shows the diffraction spectra of the examined zeolite. The parental material is identified as clinoptilolite ($(Na,K,Ca)_5Al_6Si_{30}O_{72}.18H_2O$), and its characteristic peaks were recognized at 2θ = 9.87° (*d* spacing: 8.94 Å), 22.487° (*d* = 3.95 Å) and 30.360° (*d* = 2.94 Å). The sample also contains small amounts of mica/illite, cristobalite (SiO_2), dolomite ($CaMg(CO_3)_2$) and feldspar [albite $(Na,Ca)(Si,Al)_4O_8$/anorthite $(Ca,Na)(Si,Al)_4O_8$] (possibly). The characteristic peaks found in the present study are in accordance to other studies, as shown by the comprehensive relative data of Table 8, which are typical for clinoptilolite samples. As reported by Perraki et al. [163], in heulandite, the highest peak is attributed to the (020) reflection (*d* = 8.99 Å), whereas in clinoptilolite the higher peak is attributed to the (040) reflection (*d* = 3.98 Å) [163]. The (020) reflection of heulandite at 9.9°2θ is always far more intense than the remaining lines of the pattern, while this same reflection in X-Ray tracings of clinoptilolite is, in many samples, exceeded in intensity by the (004) peak at about 22.3°2θ. The differences between diffractometer tracings of clinoptilolite and heulandite have been reported enough for distinguishing these two similar zeolites [184]. The thermal behavior of the zeolite samples in conjunction to XRD analysis, shown in Fig. 5, has been studied in a wide range of temperatures (25°C–400°C–540°C–600°C–740°C–940°C). The key difference between heulandites and clinoptilolite is their behavior upon heating. Clinoptilolite is stable at temperatures exceeding 450°C; heulandites undergo structural collapse below 450°C [160]. A partial framework breakdown indicates the presence of an intermediate member of the heulandite–clinoptilolite isomorphous series, "heulandite type-II" [163].

Table 6
Chemical analysis of minerals by XRF

	Zeolite		Bentonite		Vermiculite	
	% w/w	meq/g	% w/w	meq/g	% w/w	meq/g
SiO_2	70.1		55.9		47	
Al_2O_3	12.0		18.0		16.6	
Fe_2O_3	0.727		3.85		12.3	
CaO	3.04	1.084	3.63	1.295	0.575	0.207
MgO	0.765	0.382	3.53	1.752	21.6	10.718
Na_2O	0.304	0.097	3.52	1.136	–	–
SO_3	140 ppm		1.20		270 ppm	
TiO_2	0.113		0.706		0.922	
K_2O	3.31	0.703	0.611	0.130	0.350	0.074
P_2O_5	–		0.136		520 ppm	
Cl	52 ppm		550 ppm		–	
MnO	440 ppm		450 ppm		0.150	
BaO	–		280 ppm		210 ppm	
V_2O_5	270 ppm		280 ppm		89 ppm	
ZnO	38 ppm		49 ppm		270 ppm	
NiO	15 ppm		33 ppm		0.172	
SrO	130 ppm		32 ppm		25 ppm	
CuO	–		25 ppm		–	
Cr_2O_3	–		18 ppm		0.254	
Rb_2O	93 ppm		15 ppm		–	
ZrO_2	–		12 ppm		–	
Ag_2O	–		2 ppm		–	
PbO	13 ppm		–		–	
Co_3O_4	–		–		120 ppm	
Nb_2O_5	–		–		21 ppm	
LOI[a]	9.45		8.75		–	

[a]LOI: mass loss upon firing at 1,100°C.

3.3.2. Mineralogy of bentonite and vermiculite

The XRD pattern of the natural bentonite (Fig. 6) shows reflection peaks at about 2θ = 7.28°–13.29°–19.91°–28.5°, corresponding to a spacing of 12.13–6.66–4.46–3.13 Å. These reflections are attributed to montmorillonite, which is the main component of the mineral, with mass percentage up to ~76 wt%. Small amounts of mica/illite, dolomite (2θ = 31.120°, d = 2.87) [$CaMg(CO_3)_2$], calcite (2θ = 29.74°, d = 3) [$CaCO_3$], quartz (2θ = 26.921°, d = 3.30915) [SiO_2], anatase (2θ = 25.55°, d = 3.48) [TiO_2] and pyrite (2θ = 33.3°, d = 2.69) [FeS_2] have been also identified. Mineralogy of bentonite samples (XRD) can be connected with the chemical analysis of the mineral (XRF), and more specifically, the reflection peaks of an XRD pattern are connected to the elemental content in the structure of the mineral [164]. Perraki and Orfanoudaki [164] reported that in minerals rich in calcium (Ca-montmorillonite), the main reflection peak is d(001) ~15 Å, but when it is referred to as a sodium form (Na-montmorillonite), the corresponding peak is d(001) ~12.5 Å. Caglar et al. [143] reported that when higher d(001) distance of raw bentonites (15.33 Å) than that of Na-montmorillonite (12.04 Å) are measured and the basal spacing values varied in the range 14.45–15.40 Å, this reveals the presence of a calcium-rich bentonite sample. The d(060) peak which is often used to identify the type of smectites, when located at 1.50 Å in the XRD pattern of raw bentonite reveals an Al-rich 2:1 dioctahedral montmorillonite [143]. Tabak et al. [141] reported that after treatment with water, the reflection peaks distance is expanded and is depended on the layer charge, the size and charge of the exchangeable cations [141].

The XRD pattern of natural vermiculite (Fig. 7) shows reflection peaks at about 2θ = 6.15°–24.71°–31.05°, corresponding to a basal d spacing of 14.35, 3.59 and 2.88°Å.

Perez-Maqueda et al. [147] studied three different vermiculite samples (Mg, Na and NH_4 vermiculite) in different temperatures and showed that upon heating, interlayer distances decreased. More specifically, X-ray diffraction pattern of natural Mg^{2+} vermiculite is characterized by an interlayer distance of 14.4 Å. After heating at 125°C, 225°C and 250–650°C, the interlayer distance decreased to 11.6, 10.25 and 10 Å, respectively. In Na^+-vermiculite sample with a layer distance about 12 Å, after dehydration, the interlayer distance decreased to 9.99 Å. The NH_4^+-saturated vermiculite with an interlayer distance of 10.7 Å, when heated to 225°C and 325°C, the interlayer spacing was decreased to 10.6 and 10.54 Å, respectively [147].

Table 7
Chemical analysis and CEC of natural minerals from different origin

Mineral/country of origin	Chemical analysis (%)								CEC (meq/g)	Reference
	SiO_2	Al_2O_3	Fe_2O_3	CaO	MgO	Na_2O	K_2O	TiO_2	CEC	
Clinoptilolite										
Australia	68.26	12.99	1.37	2.09	0.83	0.64	4.11	0.23	1.20	[175]
Brazil	67.82	14.96	0.42	1.87	0.18	0.32	4.47	0.07	2.29	[175]
Greece	65.12	12.86	1.52	3.04	1.54	1.18	1.55	–	–	[56]
Greece	67.1	12.2	1.0	3.3	1.08	0.55	1.76	0.16	–	[176]
Greece	–	–	–	–	–	–	–	–	1.47	[158]
Armenian	–	–	–	–	–	–	–	–	1.36	[158]
Georgian	–	–	–	–	–	–	–	–	1.81	[158]
Iran	70.00	10.46	0.46	0.2	–	2.86	4.92	0.02	–	[175]
Iran	66.5	11.81	1.3	3.11	0.72	2.01	3.12	0.21	1.20	[175]
China	65.52	9.89	1.04	3.17	0.61	2.31	0.88	0.21	1.03	[175]
China	68.27	7.48	1.95	2.61	1.87	0.68	1.69	–	–	[175]
China	69.5	11.05	0.08	2.95	0.13	2.95	1.13	0.14	–	[175]
Cuba	62.36	13.14	1.63	2.72	1.22	3.99	1.20	–	–	[175]
Croatia	64.93	13.39	2.07	2.00	1.08	2.40	1.30	–	1.45	[175]
Croatia	55.80	13.32	1.30	5.75	0.70	3.90	2.35	–	–	[175]
Ukraine	67.29	12.32	1.26	3.01	0.29	0.66	2.76	0.26	–	[175]
Ukraine	66.7	12.3	1.05	2.10	1.07	2.06	2.96	–	0.64	[175]
Slovakia	67.16	12.30	2.30	2.91	1.10	0.66	2.28	0.17	–	[175]
Turkey	70.90	12.40	1.21	2.54	0.83	0.28	4.46	0.089	1.6–1.8	[175]
Turkey	69.72	11.74	1.21	2.30	0.31	0.76	4.14	–	1.84	[175]
Turkey	69.31	13.11	1.31	2.07	1.13	0.52	2.83	–	–	[175]
Turkey	64.99	9.99	3.99	3.51	1.01	0.18	1.95	–	–	[175]
Turkey	70.00	14.00	0.75	2.50	1.15	0.20	2.30	0.05	–	[175]
Chile	67.00	13.00	2.00	3.20	0.69	2.60	0.45	0.20	2.05	[175]
Bentonite										
Algeria	57.50	19.0	3.0	1–3	1–2	1–3	–	–	–	[177]
Germany (Mossburg)	59.42	19.08	4.64	2.14	4.72	0.08	–	0.26	–	[178]
Greece	50.01	15.39	2.98	5.98	2.55	0.68	0.33	0.25	0.97–1.12	[179]
Greece (Milos, Komia)	67.46	16.10	3.60	2.62	1.40	0.72	–	0.26	–	[178]
Greece (Milos, Trogalas)	69.98	17.09	2.16	0.96	2.18	0.44	–	0.20	–	[178]
USA (Wyoming)	64.32	20.74	3.49	0.52	2.3	2.59	–	0.14	–	[178]
USA (Mississipi)	64.00	17.10	4.7	1.5	3.8	0.2	–	–	–	[178]
Italy (Ponze)	67.42	15.83	0.88	2.64	1.09	0.30	–	–	–	[178]
Canada	61.4	18.1	3.2	0.6	2.3	2.2	0.4	0.1	0.85	[24]
Pakistan	70.68	16.22	3.21	4.62	3.0	0.71	1.05	0.33	0.77	[180]
Turkey	56.28	26.79	4.0	1.34	3.67	–	–	–	–	[181]
Turkey	60.53	15.21	4.31	4.11	2.17	3.57	0.75	–	–	[13]
Vermiculite										
Africa (North Transvaal, Africa Rochester)	44.62	9.18	5.46	0.78	20.44	0.11	0.48	–	0.94	[43]
Greece	37.62–40.26	12.39–14.79	8.16–10.50	0.17–0.36	21.19–22.27	0	0–5.30	0.65–0.91	1.48–0.94	[182]
India	40.13	17.99	8.73	–	12.04	–	9.14	–	0.62	[183]
Italy (Aldrich)	40.87	19.46	–	0.22	18.41	0.04	8.31	1.02	0.40	[39]
Italy	39.0	12.0	8.0	3.0	20.0	–	4.0	–	1.0	[45]

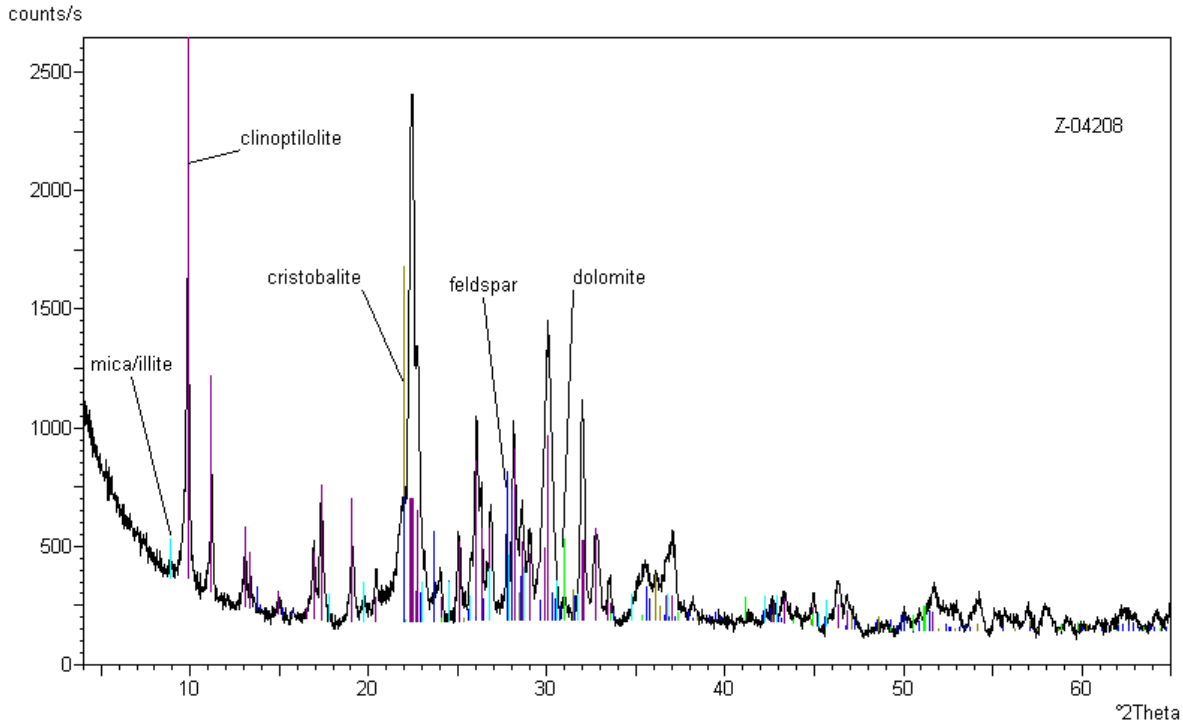

Fig. 4. XRD pattern of clinoptilolite.

Table 8
XRD data of clinoptilolite, bentonite and vermiculite

Reference	Mineral	2θ	*d* spacing (Å)
Zeolite			
[185]	Clinoptilolite	9.85–22.4–30.0	9.029–3.971–2.977
[185]	Quartz	26.8	3.347
[185]	Mica	9.00	9.990
[186]	Clinoptilolite	–	9.044–3.97–2.979
[186]	Clinoptilolite	–	8.92–3.964–2.974
[56]	Clinoptilolite M	–	9.04–3.97–2.98
[56]	Clinoptilolite Σ	–	9.00–3.96–2.97
[187]	Clinoptilolite	9.83; 10.07; 22.818	
[160,188]	Heulandite type-II	–	8.92–3.958
[160]	Cristobalite	–	4.05
[160]	Feldspar	–	3.20
[132]	Clinoptilolite	9.87–22.4–30.0	–
Present study	Clinoptilolite	9.8[a]–11.16–17.29–22.39[a]–22.8–28.17–29.98	9.01–7.92–5.12–3.96–3.89–3.16–2.97
Bentonite			
[143]	Bentonite	5.76–17.60–19.84–34.80–61.84	15.33–5.03–4.47–2.58–1.50
[143]	Quarz	20.88–26.81	4.25–3.32
[143]	Dolomite	23.43–29.83	3.79–2.99
[141]	Bentonite W	6.20	14.24
[141]	Bentonite R	7.04	12.54
[189]	Na-bentonite		*d*(001) = 14.29 Å and *d*(020) = 4.49 Å
Present study	Montmorillonite	5.4–7.36[a]–13.7–20.02–28.64	16.35–11.99[a]–6.45–4.42–3.11
Present study	Montmorillonite	7.28[a]–13.29–19.11–28.5	12.13[a]–6.65–4.45–3.12

(continued)

Table 8 *(continued)*

Reference	Mineral	2θ	*d* spacing (Å)
Present study	Montmorillonite	–	12.4[a]
Present study	Dolomite	31.12	2.87
Present study	Calcite	29.74–35.73	3.00–2.51
Present study	Quartz	26.92	3.30
Present study	Pyrite	28.63–33.3	3.11–2.68
Present study	Anatase	25.54	3.48
Vermiculite			
[149]	Vermiculite	–	14.35
[149]	Mg-Vermiculite	–	14.43
[147]	Mg-Vermiculite	–	14.4
[147]	Na-Vermiculite	–	12.16
[147]	NH_4-Vermiculite	–	10.7
[148]	Vermiculite	–	14.4
[190]	Vermiculite	–	14.1
[191]	Vermiculite	–	14.52
[38]	Vermiculite	6.03	14.65
Present study	Vermiculite	6.15[a]–12.29–18.56–24.70–31.04	14.33[a]–7.19–4.77–3.60–2.87

[a]Main peaks.

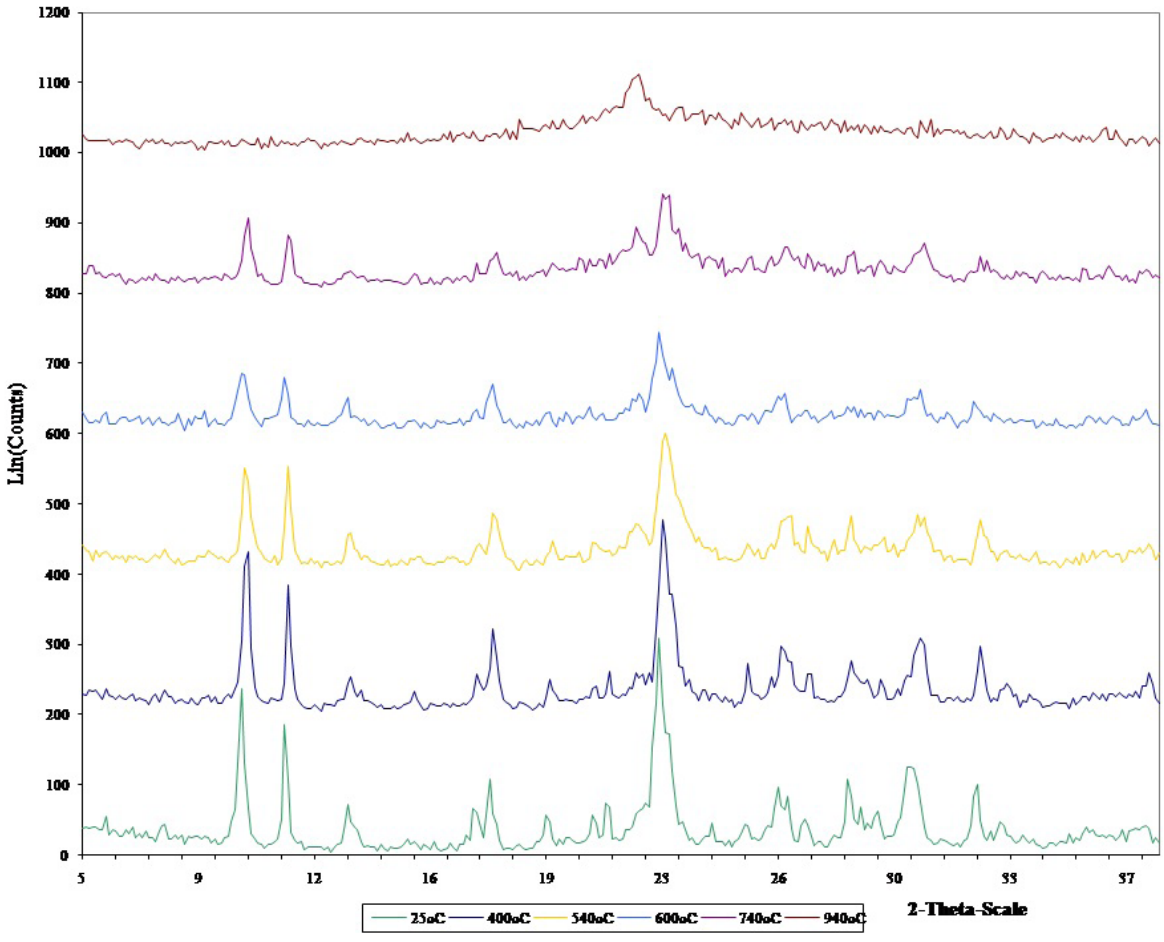

Fig. 5. XRD patterns of clinoptilolite vs. temperature pretreatment.

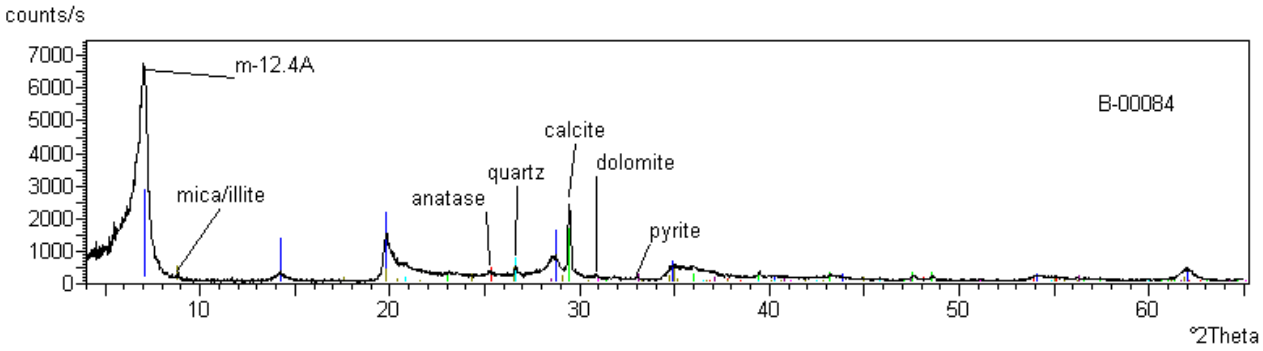

Fig. 6. XRD pattern of bentonite.

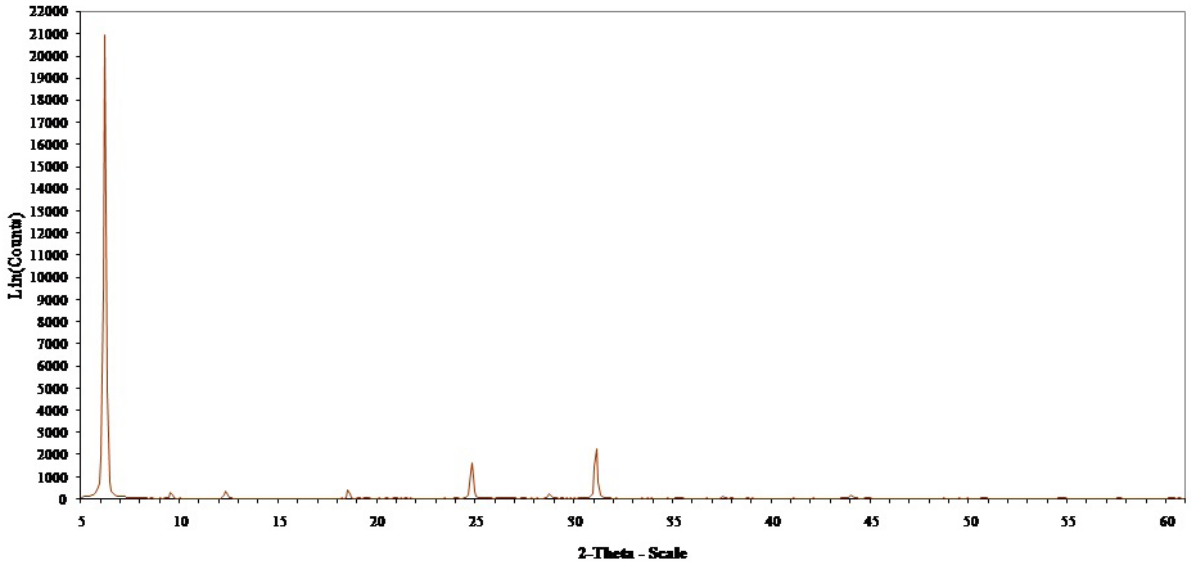

Fig. 7. XRD pattern of vermiculite.

3.4. Thermal analysis of minerals

3.4.1. Thermal characterization of zeolite

Taking into account the dehydration behavior of zeolites, they can be distinguished into two main categories, the ones that do not show major structural changes and those that undergo structural changes with dehydration [8]. According to the literature, heulandite/clinoptilolite zeolites can be classified into three different types according to their thermal behavior. According to these types, information regarding their framework contraction and reversible dehydration, irreversible structural changes, hindered rehydration and structure collapse upon heating (>450°C, >550°C, >750°C, respectively) can be obtained [8]. In general, thermal stability of a mineral increase with increasing Si/Al ratio, because more energy is required to break the Si–O bond compared with the Al–O bond [8].

Thermal characterization data for clinoptilolite reported in literature are summarized in Table 9. The TG/DTA and weight loss curves of the zeolite sample are presented in Fig. 8. The TG curve of the examined sample showed a rather continuous weight loss behavior when heated up to 700°C, due to the loss of hygroscopic water (25°C–100°C) and the loss of water residing in the channels and the cavities of the zeolite framework. The most important aspects of zeolite thermal analysis reported in literature and confirmed by the current study are summarized below:

- In the range 25°C–400°C, the endothermal (DTA diagram) process of dehydration occurs in two steps for heulandites samples, but in one step for clinoptilolites [137,163].
- Continuous TG curve and the absence of a sharp peak in the corresponding DTG curve, which indicates the transformation of heulandites-to-heulandite B at about 260°C–280°C, confirmed that the major constituent of the sample is clinoptilolite rather than heulandite [77,192].
- The dehydration process is characteristic of the weight loss in a TG curve and of the endothermal peak in a DTA and DTG curve, in the range of 25°C–700°C.
- The process of dehydration, occurring in two separated steps, corresponds to the classification of water into two groups according to its bond strength with cations. Regarding channels, first leaves the weakly bonded

Table 9
TG/DTA literature data

Reference		Temperature range °C	Loss of mass (% w/w)	Endothermic peak (°C)	Reason	Exothermic peak (°C)	Reason
Zeolite							
[129]	Clinoptilolite	20–1,000	10.91	100–105 140–142 250–260	Water loss	–	–
	Pb-clinoptilolite					300–350	Ammonia complexes
[130]	NH_4-clinoptilolite	20–750	–	20–230	Desorption of zeolitic water	230–350	Desorption and oxidation of ammonia
				620–640	Dehydroxylation reaction	340–350	Decomposition of strongly bonded NH_4^+
[131]	Zeolite	100–450	12–15	70	Dehydration/dehydroxylation		
				180	Dehydration		
		600–800	1–1.5	1,000	Collapse of zeolite structure and formation of amorphous phase	400–900	Structural changes
[132]	Clinoptilolite	30–1,000	11.72–11.98	125–135	Dehydration	–	–
[192]	Zeolite	23–1,000	14	140	Dehydration	–	–
				260	Transformation of normal heulandites to heulandites B		
				360	Slow structural water elimination of zeolite		
				690	Structural change of clinoptilolite		
[135]	Clinoptilolite	25–1,000	12.08	100	Dehydration	–	–
				200	Dehydroxylation		
[136]	Zeolite-Na	25–1,025	15.58	85.2(DTG)	Water loss due to weakly bound water	833 (DSC)	Exothermic transformation
				174.5(DTG)	Weight loss due to the water located in cavities and bound to the non-framework cations		
				472.3(DTG)	Due to structural water and to the destruction of zeolite structure		
	Zeolite-K	25–1,025	14.33	71 (DTG)	Water loss due to weakly bound water	838.8 (DSC)	Exothermic transformation
				171 (DTG)	Weight loss due to the water located in cavities and bound to the non-framework cations		
				491.7 (DTG)	Due to structural water and to the destruction of zeolite structure		

(continued)

Table 9 *(continued)*

Reference		Temperature range °C	Loss of mass (% w/w)	Endothermic peak (°C)	Reason	Exothermic peak (°C)	Reason
	Zeolite-NH_4	25–1,025	15.26	62.5 (DTG) 186.3 (DTG) 473 (DTG) 483.3 (DSC)	Water loss due to weakly bound water Weight loss due to the water located in cavities and bound to the non-framework cations Due to structural water and to the destruction of zeolite structure Due to the desorption and decomposition of the ammonium ion	687.3 (DTG) 829.1 (DSC)	Exothermic transformation
	Zeolite-Zn	25–1,025	17.32	97.4 (DTG) 224.9 (DTG) 462.5 (DTG)	Water loss due to weakly bound water Weight loss due to the water located in cavities and bound to the non-framework cations Due to structural water and to the destruction of zeolite structure	836.5 (DSC)	Exothermic transformation
	Zeolite-Pb	25–1,025	14.16	71.2 (DTG) 221.1 (DTG)	Water loss due to weakly bound water Weight loss due to the water located in cavities and bound to the non-framework cations	829.6 (DSC)	Exothermic transformation
[193]	Zeolite	20–1,100	9.6	117.3 642.1	Dehydration Dehydroxylation	924.2	Collapse of the structure
[139]	NaY-zeolite	–	–	127	Dehydration	882	Collapse
[8]	Clinoptilolite-Na	–	–	~30–230	Dehydration	~920	Collapse
	Clinoptilolite-K	–	–	~200	Dehydration	~1,000	Collapse
	Clinoptilolite-Cs	–	–	~50–200	Dehydration	~1,070	Collapse
	Clinoptilolite-Ca	–	–	140–400	Dehydration	~900	Collapse
	Heulandite-K	–	–	~100–300	Dehydration	>300	Collapse
	Heulandite-Ca + Na	–	–	~360	Dehydration	>360	Collapse
	Heulandite-Ca + K	–	–	~175	Dehydration	>175	Collapse
	Heulandite-Sr	–	–	~100–270	Dehydration	<270	Collapse
	Heulandite-Cd	–	–	~50–200	Dehydration	>250	Collapse
[134]	Ca-Clinoptilolite	20–200 200–700	6.7 5.8	113; 192; 348; 404 (DTG)	Dehydration	484 (DTA)	Pyrite oxidation

(continued)

Table 9 *(continued)*

Reference		Temperature range °C	Loss of mass (% w/w)	Endothermic peak (°C)	Reason	Exothermic peak (°C)	Reason
[133,163]	Heulandite-II	25–100	3.96		Loss of hydroscopic water	–	–
		100–200	4.01	200	Loss of loosely bonded water		
		200–300	2.32	360	Dehydration		
		300–400	1.72		Dehydration		
		400–500	0.95		Dehydration		
		500–600	0.62				
		600–1,000	0.52				
Bentonite							
[143]	Bentonite	25–129	8.1	99	Elimination of water coordinated to the		
		129–220	3.1	166	interlayer cations	910	Decomposition of dolomite impurity
		300–720	4.3	509; 658	Elimination of water coordinated to the		
		720–950	0.0		interlayer cations		
					Dehydroxylation of amorphous smectites		
	Na-bentonite	30–290	8.9	64	Dehydration (single step process)	–	–
		290–830	4.3	638	Dehydroxylation		
	Ca-bentonite	28–115	9.9	63	Dehydration	–	–
		115–174	2.9	140	Dehydration		
		290–770	4.1	647	Dehydroxylation		
	Pb-bentonite	30–290	10.0	69	Dehydration	918	Development of cristobalite and mullite
		290–780	3.9	626	Dehydroxylation		
	Cu-bentonite	30–300	10.7	78	Dehydration (adsorbed and cation coordi-	–	–
		300–460	1.1	369	nated water)		
		460–600	1.6	577	Dehydroxylation		
		600–870	1.7	630	Dehydroxylation		
					Dehydroxylation		
	Zn-bentonite	30–280	12.4	62	Dehydration	–	–
		280–850	4.2	618	Dehydroxylation		
[141]	Resadiye bentonite	24–123	5.90	57	Dehydration	–	–
		210–587	2.30	686	Dehydroxylation		
		587–720	3.80				
	Wyoming bentonite	30–160	5.65	79	Dehydration	–	–
		550–742	3.30	673	Dehydroxylation		
[144]	Bentonite	20–193	5.15	55; 126; 193	Loss of bulk and interlayer water	–	–
		566–739	3.25	686	Dehydroxylation of lattice water		
[142]	Bentonite	20–200	18.3	91.8	Dehydration of interlayer and surface	360.4	–
		200–400	2.0	627.9	water		
		400–800	2.9		Dehydroxylation		

(continued)

Table 9 *(continued)*

Reference		Temperature range °C	Loss of mass (% w/w)	Endothermic peak (°C)	Reason	Exothermic peak (°C)	Reason
[145]	Bentonite	25–400	8.8	80; 148	Dehydration of interparticle, adsorbed		
		400–800	4.6	672	and interlayer water	980	Decrystallization of CaS
		800–1,100	0.4		Dehydroxylation	1,029	Recrystallization of new phases
[140]	Bentonite	100–400	~9	~50	Dehydration		
		600–800	~2	~700	Dehydroxylation	~650	Recrystallization
		950–1,050				~1,010	Loss of crystal structure of the 2:1 layers and recrystallization
Vermiculite							
[151]	Untreated vermiculite	25–1,200	–	220	Dehydration	–	–
	Ground vermiculite	25–1,200	–	100–450	Dehydration	–	–
[152]	Mg-vermiculite	30–300	~15	125	Dehydration		
				200–250	Dehydration, molecules in intermediate	700–850	Formation of enstatite
				>650	contact with Mg ions		
					Dehydroxylation		
	Na-vermiculite	25–1,000	~13	110	Dehydration	850–975	Formation of enstatite
				>400	Dehydroxylation		
	NH_4-vermiculite	25–1,000	~0.14	40–200	Loss water from voids	600–830	Release of ammonia
						730–830	Annealing of structure irregularities
[146]	Pure vermiculite	25–1,000	–	140–150	Dehydration		
				260–270	Dehydration	910	–
				875			
	Mg-vermiculite	25–1,000	–	110	Dehydration (characteristic of		
				205	Mg-vermiculites)	890	–
				575	Dehydration (characteristic of		
				850	Mg-vermiculites)		
					Dehydroxylation		
[148]	Vermiculite	25–1,000	–	100–250	Loss of interlayer water	–	–
				500–600	Loss of water due to a breakdown of	800–900	Formation of clinoenstatite
				700–900	the octahedral cation to hydroxyl bond		
[149]	Mg-vermiculite	25–180	9.87	150	Loss of interlayer water		
		180–300	4.45	260	Dehydroxylation of OH groups	920	Transformation to enstatite
		620–940	4.60	820; 890	coordinated to Mg ions		
					Dehydroxylation		
[150]	Vermiculite	25–1,000	~13	<300	Loss of interlayer water	–	–
				~550	Dehydroxylation		
				~700	Loss of hydroxyl groups of the 2:1 layer		
[152]	Vermiculite	25–200	9.7	110	Dehydration	–	–
		200–450	5.1		Dehydration		
		550–750	5.4		Dehydroxylation		

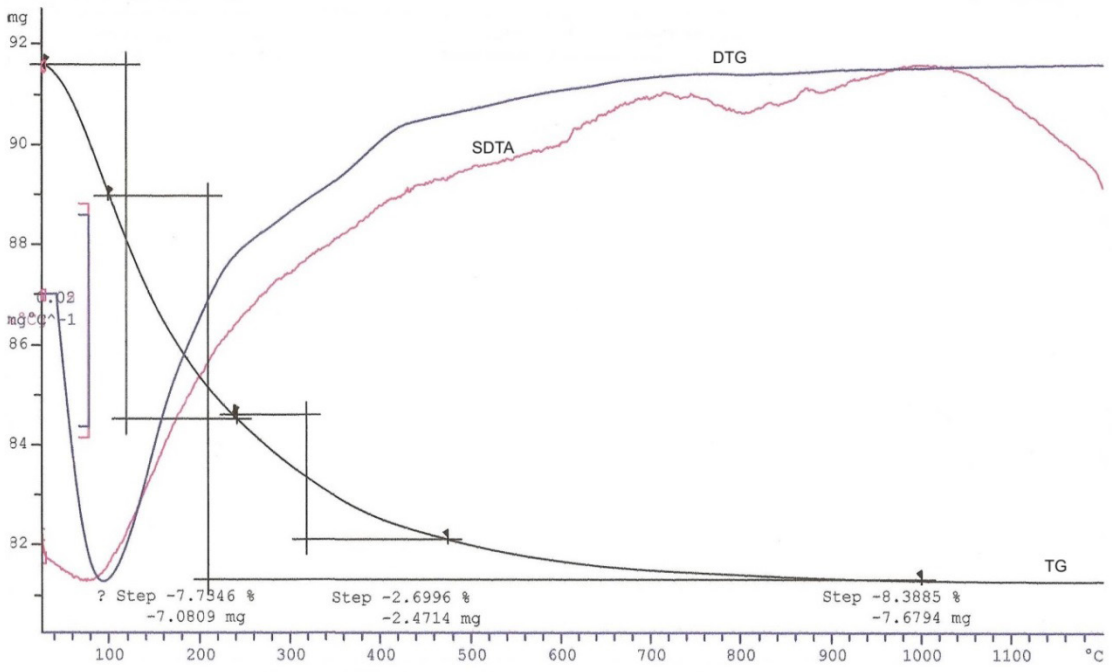

Fig. 8. TG/DTA curves for clinoptilolite.

water, whose content varies with the type of cation and the degree of occupancy of particular cationic sites. The water molecules strongly bonded with cations leave at a higher temperature [137].

- At the beginning of the heating process and up to 200°C the recorded weight loss corresponds to weakly bound water. The weight loss at between 250°C and 400°C is attributed to the dehydroxylation reaction ($2OH^- \rightarrow O^{2-} + H_2O$), and it occurs for solids which contain structural OH. There is also a third weight loss region (450°C–500°C), which corresponds to structural water and to the destruction of zeolitic structure [135].
- Perraki and Orfanoudaki [133] reported that in thermal studies of zeolite, for different grain fractions of the mineral, the weight loss of >63 μm fraction is 8.21%, while that of <2 μm fraction is 10.02%. This difference is due to the fact that the >63 μm fraction also contains minerals that do not lose weight upon heating, such as cristobalite and quartz [133].
- The zeolite water loss was higher in the zeolites exchanged with bivalent ions. Further, in the monovalent and bivalent ions, the larger cations had less zeolite water loss (sum of the weakly bound water and metal bound), since the greater is the size of the non-framework cation, the smaller is the space for the zeolite water [136].
- In the range of 400°C–1,000°C, several exothermic peaks can be observed in DTA and DTG curves, which correspond to transformations or even collapse of the crystal structure of the zeolites. Vujakovic et al. [134] reported that the peak at 484°C is characteristic of the oxidation of pyrite [134].
- In the literature, DTA curves of heulandites show an endothermic reaction at 200°C, followed by a stronger endothermic peak at 360°C, while the DTA curves of clinoptilolites show a broad endothermic peak at around 90°C–200°C [163]. If the differences in thermal stability between heulandites and clinoptilolite are solely due to the nature of the exchangeable cation in each species, one might expect a calcium-exchanged clinoptilolite to exhibit the low temperature reactions and the low thermal stability of heulandite. Inversely, a sodium-exchanged heulandite should be more thermally stable than the calcium variety [184].
- Exothermic peaks can be also found lower than 400°C, attributed to the desorption and oxidation of NH_4 [129,130].

3.4.2. Thermal characterization of bentonite

Thermal characterization data for bentonite reported in literature are summarized in Table 9. The most important observations regarding bentonite thermal analysis (Fig. 9) are summarized as follows:

- In most DTA curves, some endothermic peaks are observed between 100°C and 400°C, which is the result of dehydration. The endothermic peak, which results from dehydroxylation and the exothermic peak that results from recrystallization are observed at 600°C–800°C. The exothermic peak resulting from the loss of the crystal structure of the 2:1 layers of calcium-montmorillonite (CaM) and recrystallization is observed at 950°C–1,050°C [140].
- Tabak et al. [141] reported that the noticeable differences between the mass losses of two untreated bentonites (Wyoming and Resadiye) in the temperature interval 210°C–550°C, are attributed to the existence of external clay components such as dolomite, α-cristobalite, quartz, calcite, and illite of Resadiye bentonite [141].

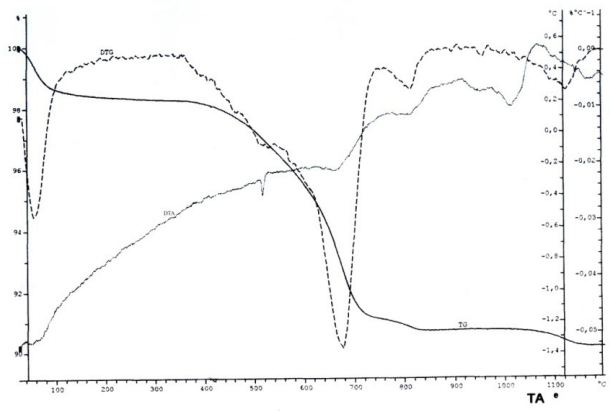

Fig. 9. TG/DTA curves for bentonite.

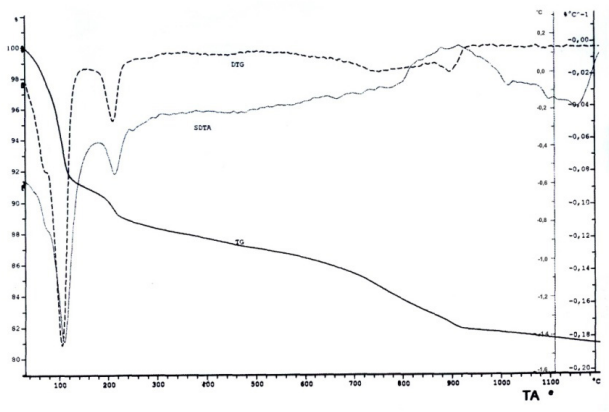

Fig. 10. TG/DTA curves for vermiculite.

- Above 900°C, all major structural changes result in the development of cristobalite and mullite in montmorillonite [143].
- Caglar et al. [143] reported that the dehydration of Na-bentonite occurs in the temperature range of 30°C–290°C as a single-step (same for Pb, Cu and Zn-bentonite) process, which gives rise to an endothermic maximum, whereas the same process takes place in two stages for raw bentonite [143].

3.4.3. Thermal characterization of vermiculite

Thermal characterization data for vermiculite reported in literature are summarized in Table 9. The most important aspects of the current vermiculite thermal analysis (Fig. 10) are summarized below:

- Pure vermiculites show large endothermic effects at 145°C–150°C with smaller ones at 260°C–270°C and correspond to Mg-vermiculites. Some samples show a small endothermic effect at about 550°C and a corresponding weight loss on the TG curve, which are attributed to dehydroxylation of mica present in vermiculite. Other samples show two endothermic effects at 110°C and 205°C which are characteristic of Mg-vermiculites. Weight loss on the TG curve associated with the endothermic effect at 575°C may be attributed to dehydroxylation of partially altered mica comprising this interstratification [146,149].
- Pretreated vermiculites, such as ground vermiculites, give different thermal curves than raw vermiculite [151].
- The exothermic peaks in DTA curve are due to: 600°C–830°C release of ammonia, 700°C–850°C and 850°C–975°C formation of enstatite [149], 800°C–900°C formation of clinoenstatite [148].

3.5. Capacity measurements

Ion-exchange capacity is one of the most important parameters of natural silicate minerals and is connected to the level of undergoing ion exchange. It can be measured as the sum of the exchangeable cations that can be bonded by the mineral framework, and is expressed in meq/g (Table 7) [133]. Isomorphous substitutions of Al to Si in the tetrahedral framework and the open tectosilicate structure are the cause of ion-exchange capacity. In Table 10, the measured mineral capacities are provided. According to the mineral supplier, the mean value of CEC is equal to 1.88 meq/g for clinoptilolite and 1 meq/g for bentonite. Kantiranis et al. [179] reported that bentonite deposits in Greece have a capacity between 0.97 and 1.12 meq/g, with a mean value of 1.04 meq/g for bentonite deposits of Milos and 0.90–1.30 meq/g for bentonite deposits from Milos Aggeria [179].

TEC is the total sum of the mineral exchangeable cations. The combined concentration of exchangeable cation oxides (MgO + CaO + Na_2O + K_2O) for the examined samples is: 7.4 wt% for clinoptilolite, 11.3 wt% for bentonite and 22.5 wt% for vermiculite. It has to be noted that there is a great difference between the structure of zeolites (tectosilicates) and smectite and vermiculite (2:1 phyllosilicates). Mg is mainly a structural cation, that is, not exchangeable cation, in both smectite (montmorillonite) and vermiculite. So the exchange capacity of those has to be greater than the sum of CaO + Na_2O + K_2O, which in the present case is 2.561 for montmorillonite and 0.281 for vermiculite.

In several literature sources, it is stated that the capacity of the two investigated clays is similar; in reality there is some differentiation, mainly attributed to the value of the oxides of the bivalent cations (Ca/Mg) and to the different places of the cations placed into the crystal structure of the two minerals. Bentonite has a ratio of Ca/Mg equal to 0.74, whereas in vermiculite the same ratio is equal to 0.019. It is noted that bentonite presents elevated concentrations of Na_2O and K_2O compared with vermiculite. Calcium ions in bentonites (montmorillonite) are usually hydrated and weakly bound into the structure of the mineral, which makes them easily replaceable by other cations. Further, Mg in clay minerals is more difficult to exchange compared with calcium, and this make clays with high Ca concentration to present higher ion-exchange capacities than those rich in magnesium ions [179].

3.6. Porosimetric and microstructural investigations

Natural zeolites are characterized by primary and secondary porosity. The primary porosity (microporosity <20 Å or <2 nm) results from the specific crystalline structure of the zeolite particles, which in turn depends upon its composition. Matrix inserted between zeolite particles causes secondary porosity, that is, the presence of transitional

Table 10
Mineral ion-exchange capacities

Capacity (meq/g)	Clinoptilolite	Bentonite	Vermiculite
TEC	<2.266	<4.312	<11.00
MEL			
Pb	1.668 ± 0.122	2.667 ± 0.310	1.974 ± 0.341
Cu	0.856 ± 0.144	2.600 ± 0.491	1.699 ± 0.079
Zn	0.821 ± 0.244	2.607 ± 0.083	1.335 ± 0.113
Mn	0.575 ± 0.019	2.336 ± 1.065	1.246 ± 0.032
Cr	0.829 ± 0.124	3.398 ± 0.585	2.019 ± 0.280

(20–200 Å) and macropores (>200 Å) [4,174]. The adsorption/desorption isotherm curves of N_2 at normal boiling temperature are used for the understanding of the textural properties of porous materials [4]. As it has been mentioned, the heterogeneity parameter (*n)* shows a dependence on the microporous structure of solids and in particular on the breadth of the pore distribution; the more homogeneous the pores are (decreased breadth), the greater its value. Porosimetric measurements can be used to obtain this type of information: Figs. 11(a)–(c) and Table 11 show the N_2 porosimetry results for the tested minerals [15], whereas Table 12 presents reference data. Upon observing Figs. 11(a)–(c), it becomes evident that the discussed minerals refer to Type IV isotherms. This type of isotherm exhibits a hysteresis loop, which is associated with capillary condensation taking place in mesopores, and has a limited uptake over a range of high P/P_0. The initial part of Type IV isotherm is attributed to a monolayer–multilayer adsorption, since it follows the same path as the corresponding part of a Type II isotherm obtained with the given adsorptive on the same surface area of the adsorbent in a non-porous form. Type IV isotherms are characteristic of many mesoporous industrial adsorbents [15].

It is well known that the heterogeneity parameter (*n*) is characteristic of the adsorbent and it is related to its structure. However, (*n*) values depend on both the adsorbate and the adsorbent and it is very difficult to have a universal exponent [194,195]. For adsorption on zeolites, (*n*) values greater than 4 have been proposed [196]. It is well known that hysteresis loops are connected to pore structure. All three materials follow similar hysteresis loop patterns, in particular of H3 type. According to IUPAC classification, this type of loop is usually given by the aggregates of platy particles or adsorbents containing slit-shaped pores. The presence of a broad hysteresis loop at the desorption isotherms (Fig. 11(a)) reveals the existence of limited-order mesoporosity–macroporosity and in the case of clinoptilolite, the inclusion of layered materials such as clays (Fig. 11(b)). However, the disordered pores may be considered a pore network with a rather undefined structure. It is interesting to note that for clinoptilolite, the most probable hysteresis loop is H1, which is produced by adsorbents having a narrow distribution of uniform pores. Indeed, pure clinoptilolite pores come in regular arrays and have a very uniform size, which is typically lower than approximately 10 Å. However, it should be mentioned that natural clinoptilolite samples contain various impurities and very rarely found in pure form. Thus, their pore structure

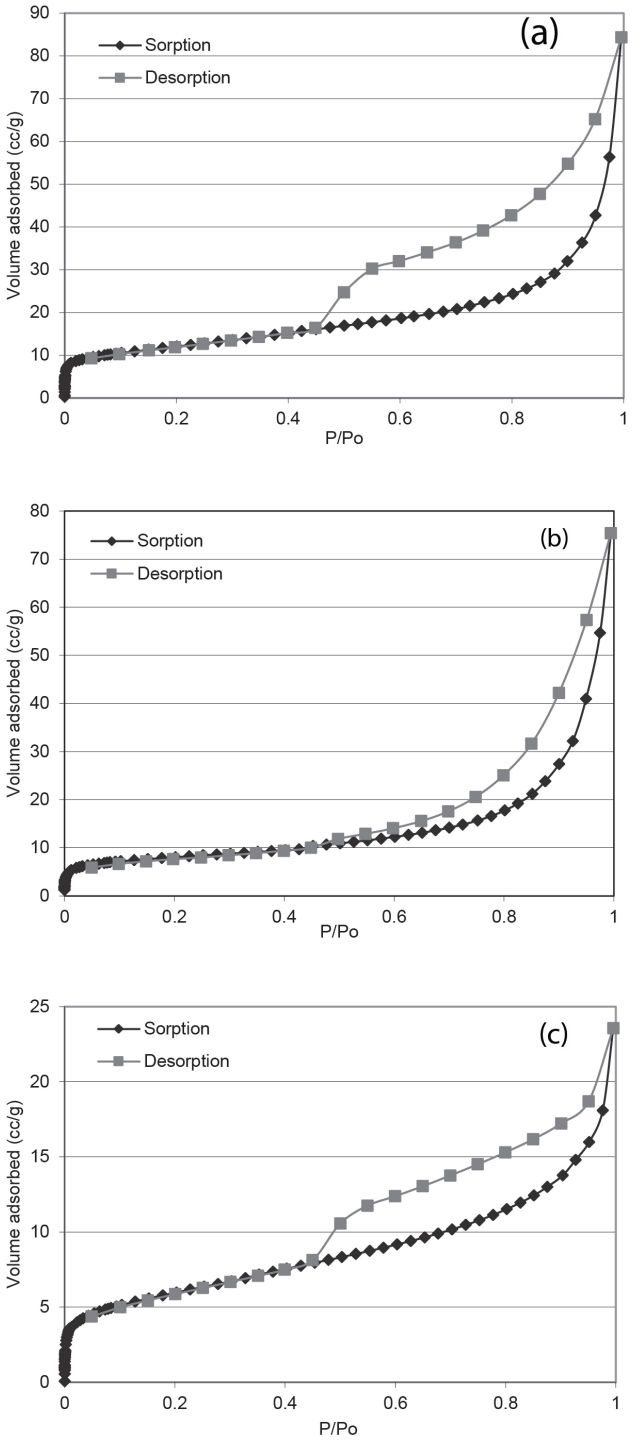

Fig. 11. N_2 sorption–desorption isotherm curves of (a) bentonite, (b) clinoptilolite and (c) vermiculite.

consists of micropores, mesopores as well as macropores of several materials giving rise to an overall disordered mesopore and macropore structure. The hysteresis loop of desorption branch for clinoptilolite is less distinct compared with bentonite and vermiculite, indicating the existence of larger pores and a more open surface area. As expected, the slit-shaped pores of clays (bentonite and vermiculite) are also in

line with the H3 hysteresis type, as observed in the nitrogen adsorption isotherms, shown in Figs. 11(a) and (c). Finally, in the case of vermiculite the different pattern in the curves for $0.9 < P/P_0 < 1$ could be interpreted as H4 hysteresis loop. Fig. 12 shows that the breadth of pore distribution follows a decreasing order as follows: bentonite > zeolite > vermiculite. Thus, the expected decreasing order of the heterogeneity parameter is the following: vermiculite > zeolite > bentonite. A difference between these materials is that clinoptilolite pores tend to group in two regions, that is, small mesopores (around 2 nm) and larger ones (around 5 nm). Similar results have been observed elsewhere [15]. Regarding the microstructure of the examined materials, they demonstrate well-formed plate or lath crystals in all cases.

4. Conclusions

The experimental results of three common natural silicate minerals – one zeolite (clinoptilolite) and two clays (bentonite and vermiculite) – are presented and compared with literature. The methods used for their structural characterization are XRD, XRF, FTIR spectroscopy, TG/DTG/DTA and N_2-porosimetry (BET). Concerning XRD, the most intense reflection in clinoptilolite corresponds to the *d*-spacing at the asymmetric position 3.97–3.98 Å plane, typical of most minerals of this type. Bentonite is mostly composed of montmorillonite, which has its characteristic features at *d*(001) = 14.29 Å and *d*(020) = 4.49 Å. The XRD pattern of natural vermiculite shows the reflection peaks at about 2θ: 6°, 24° and 31°,

Table 11
N_2 porosimetry analysis results

		Clinoptilolite	Bentonite	Vermiculite
BET	BET area [S_{BET} (m^2/g)]	28.64	41.87	20.82
	BET C[a]	375.675	583.216	216.720
	Vm[b]	6.574	9.613	4.779
Langmuir	Area (m^2/g)	28.18	38.12	23.44
	Micropore volume (mL)	0.01	0.014	0.0083
	Microporosity	0.023	0.030	0.019
	TPV[c] (mL)	0.085	0.087	0.028
	Porosity (%)	16.3	16.7	6.1

[a]BET C: dimensionless constant that is related to the enthalpy of adsorption of the adsorbate gas on the powder sample [calculated as (slope/intercept) + 1].
[b]Vm: volume of gas adsorbed at standard temperature and pressure (STP), to produce an apparent monolayer on the sample surface, in milliliters [calculated as 1/(slope + intercept)].
[c]TPV: total pore volume (mL).

Table 12
Literature BET analysis data

Mineral	BET area (m^2/g)	Type of isotherm	Mean diameter of pores (Å)	Reference
Clinoptilolite				
Clinoptilolite	31.0	Type III	<20	[135]
Clinoptilolite	17.1	Type II	–	[158]
Heulandite	19.6	Type II	–	[158]
Heulandite	16.8	Type II	–	[158]
Clinoptilolite	60	Type II	–	[132]
Clinoptilolite-Na	54	Type II	–	[132]
Clinoptilolite-K	96	Type II	–	[132]
Clinoptilolite-Ca	29	Type II	–	[132]
Clinoptilolite	14	Type IV	90	[132]
Bentonite				
Bentonite	42	Type II	30	[145]
Bentonite	35	Type II	–	[145]
Bentonite-Na	22	Type II	–	[145]
Bentonite-Ca	31	Type II	–	[145]
Vermiculite				
Vermiculite-Mg	7.1	Type II	–	[151]
Vermiculite-Na	11.6	Type II	–	[151]
Vermiculite-K	17.8	Type II	–	[151]

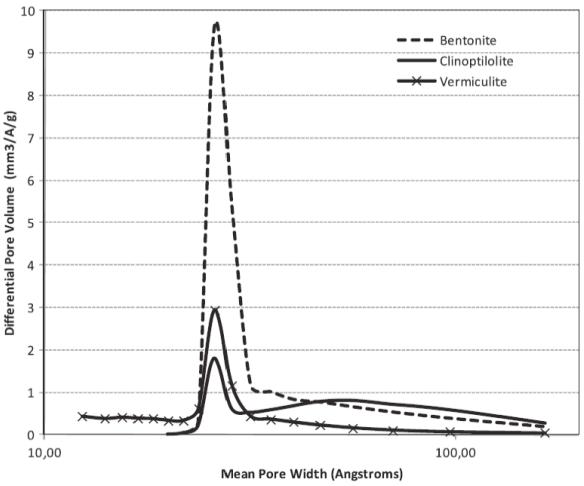

Fig. 12. Pore size distribution graph.

which correspond to the spacing $d(002)$ = 1.43, $d(008)$ = 0.48 and $d(010)$ = 0.288, respectively. FTIR analyses show that clinoptilolite exhibits characteristic water bands centered at 3,444 and 16,737 cm^{-1}. The asymmetric stretching vibration of T–O bonds in the tetrahedral sites corresponds to the band at 1,067 cm^{-1}. In bentonite, the absorption peaks group lies between 3,620 and 3,404 cm^{-1}, which is due to Al(Mg)–O–H stretching and stretching vibration bands (–OH) of water, respectively. The other peak bands at 460 and 1,031 cm^{-1} were attributed to Si–O–Si and Si–O bending vibrations, respectively. In vermiculite, the main absorption band appears at 3,387 cm^{-1}, which is characteristic of the stretching vibrations of the surface structural hydroxyl groups, whereas the bands around 996–957 cm^{-1} correspond to Si–O–Si stretching vibrations. XRF chemical analysis demonstrates that clinoptilolite Si/Al ratio is always higher than 4, while exchangeable cation oxides (MgO + CaO + Na_2O + K_2O) generally varies from 6 to 13 wt%. In bentonite and vermiculite, Si/Al ratio is normally less than 4 which is typical for heulandites as well. Typical characteristics of vermiculite include K_2O content ranging from 0 to 3 wt% and high Mg concentrations (>15 wt%). XRF analysis shows that vermiculite sample is rich in MgO (Mg-vermiculite) and the low concentration of K_2O revealed the presence of vermiculite instead of hydrobiotite. TGA shows that the main regions of clinoptilolite weight loss are the release of loosely bound water (50°C–200°C), release of "zeolitic" water (200°C–700°C) and finally collapse of crystal structure (700°C–900°C). The key difference between heulandite and clinoptilolite is their behavior upon heating. Clinoptilolite is stable at temperatures exceeding 450°C, where heulandites undergo structural collapse below 450°C. Furthermore, in the range 25°C–400°C, the endothermal (DTA diagram) process of dehydration occurred in one step which reveals the presence of clinoptilolite, because for heulandites dehydration occurs in two steps. In the case of bentonite, the adsorbed water is typically released at about 130°C, while weight loss at 525°C and between 600°C and 1,200°C are attributed to surface dehydroxylation, resulting in two endothermic peaks of absorbed water and crystallinity water losses. Dehydration of natural vermiculite occurs in two steps in the range of 30°C–300°C; the first step (up to 125°C) refers to the release of physically adsorbed water molecules, that are not in the contact with sample ions, whereas the second step (up to 200°C–250°C) refers to the release of water molecules intermediately contacting mineral ions. As far as porosity is concerned, all three minerals are generally dominated by micro/mesopores. BET surface area for clinoptilolite is between 17 and 100 m^2/g, for bentonite 22–42 m^2/g and for vermiculite 7–18 m^2/g. The above analytical results enabled the full characterization of the examined minerals, despite their common properties.

References

[1] X. Querol, J.C. Umaña, F. Plana, A. Alastuey, A. Lopez-Soler, A. Medinacelli, A. Valero, M.J. Domingo, E. Garcia-Rojo, Synthesis of zeolites from fly ash at pilot plant scale. Examples of potential applications, Fuel, 80 (2001) 857–865.

[2] M. Olivares-Marín, T.C. Drage, M.M. Maroto-Valer, Novel lithium-based sorbents from fly ashes for CO_2 capture at high temperatures, Int. J. Greenhouse Gas Control, 4 (2010) 623–629.

[3] R. Juan, S. Hernández, J.M. Andrés, C. Ruiz, Ion exchange uptake of ammonium in wastewater from a Sewage Treatment Plant by zeolitic materials from fly ash, J. Hazard. Mater., 161 (2009) 781–786.

[4] V.J. Inglezakis, A. Zorpas, Natural Zeolites Handbook, Bentham Science Publishers, Sharjah, United Arab Emirates 2012.

[5] B.B. Mamba, N.P. Dlamini, D.W. Nyembe, A.F. Mulaba-Bafubiandi, Metal adsorption capabilities of clinoptilolite and selected strains of bacteria from mine water, Phys. Chem. Earth Parts A/B/C, 34 (2009) 830–840.

[6] D.D. Pelot, S. Jun, A.L. Yarin, Bentonite dispersions: transition from liquid-like to solid-like behavior and cracking, J. Non-Newtonian Fluid Mech., 219 (2015) 50–64.

[7] M. Valášková, G.S. Martynková, Vermiculite: Structural Properties and Examples of the Use, M. Valášková, G.S. Martynková, Eds., Clay Minerals in Nature – Their Characterization, Modification and Application, E-Publishing Inc., InTech, Rijeka, Croatia 2012, pp. 209–238.

[8] G. Cruciani, Zeolites upon heating: factors governing their thermal stability and structural changes, J. Phys. Chem. Solids, 67 (2006) 1973–1994.

[9] V. Masindi, M.W. Gitari, H. Tutu, M. DeBeer, Efficiency of ball milled South African bentonite clay for remediation of acid mine drainage, J. Water Process Eng., 8 (2015) 227–240.

[10] V. Masindi, M.W. Gitari, The potential of ball-milled South African bentonite clay for attenuation of heavy metals from acidic wastewaters: simultaneous sorption of Co^{2+}, Cu^{2+}, Ni^{2+}, Pb^{2+}, and Zn^{2+} ions, J. Environ. Chem. Eng., 3 (2015) 2416–2425.

[11] F. Barbier, G. Duc, M. Petit-Ramel, Adsorption of lead and cadmium ions from aqueous solution to the montmorillonite/water interface, Colloids Surf., A, 166 (2000) 153–159.

[12] R. Naseem, S.S. Tahir, Removal of Pb(II) from aqueous/acidic solutions by using bentonite as an adsorbent, Water Res., 35 (2001) 3982–3986.

[13] R. Donat, A. Akdogan, E. Erdem, H. Cetisli, Thermodynamics of Pb^{2+} and Ni^{2+} adsorption onto natural bentonite from aqueous solutions, J. Colloid Interface Sci., 286 (2005) 43–52.

[14] O. Abollino, A. Giacomino, M. Malandrino, E. Mentasti, Interaction of metal ions with montmorillonite and vermiculite, Appl. Clay Sci., 38 (2008) 227–236.

[15] V.J. Inglezakis, M. Stylianou, M. Loizidou, Ion exchange and adsorption equilibrium studies on clinoptilolite, bentonite and vermiculite, J. Phys. Chem. Solids, 71 (2010) 279–284.

[16] A.R.A. Usman, Y. Kuzyakov, K. Stahr, Effect of clay minerals on extractability of heavy metals and sewage sludge mineralization in soil, Chem. Ecol., 20 (2004) 123–135.

[17] S. Malamis, E. Katsou, M. Stylianou, K.J. Haralambous, M. Loizidou, Copper removal from sludge permeate with ultrafiltration membranes using zeolite, bentonite and vermiculite as adsorbents, Water Sci. Technol., 61 (2010) 581.

[18] W. Wang, B. Zheng, Z. Deng, Z. Feng, L. Fu, Kinetics and equilibriums for adsorption of poly(vinyl alcohol) from aqueous solution onto natural bentonite, Chem. Eng. J., 214 (2013) 343–354.
[19] C. Maqueda, M. dos Santos Afonso, E. Morillo, R.M. Torres Sánchez, M. Perez-Sayago, T. Undabeytia, Adsorption of diuron on mechanically and thermally treated montmorillonite and sepiolite, Appl. Clay Sci., 72 (2013) 175–183.
[20] Z. Pengfei, W. Xiaoyong, G. Jiayuan, L. Xiaobing, L. Dengkui, D. Hui, Immobilization and recovery of uranium(VI) using Na-bentonite from aqueous medium: equilibrium, kinetics and thermodynamics studies, J. Mol. Liq., 209 (2015) 358–366.
[21] S. Yuebing, L. Ye, X. Yingming, L. Xuefeng, W. Lin, In situ stabilization remediation of cadmium (Cd) and lead (Pb) co-contaminated paddy soil using bentonite, Appl. Clay Sci., 105–106 (2015) 200–206.
[22] C.V. Iborra, G. Cultrone, P. Cerezo, C. Aguzzi, M.T. Baschini, J. Vallés, A. López-Galindo, Characterisation of northern Patagonian bentonites for pharmaceutical uses, Appl. Clay Sci., 31 (2006) 272–281.
[23] S. Yang, C. Han, X. Wang, M. Nagatsu, Characteristics of cesium ion sorption from aqueous solution on bentonite- and carbon nanotube-based composites, J. Hazard. Mater., 274 (2014) 46–52.
[24] T. Viraraghavan, A. Kapoor, Adsorption of mercury from wastewater by bentonite, Appl. Clay Sci., 9 (1994) 31–49.
[25] C. Karagüzel, T. Çetinel, F. Boylu, K. Çinku, M.S. Çelik, Activation of (Na, Ca)-bentonites with soda and MgO and their utilization as drilling mud, Appl. Clay Sci., 48 (2010) 398–404.
[26] S. Opaliński, M. Korczyński, M. Szołtysik, Z. Dobrzański, R. Kołacz, Application of aluminosilicates for mitigation of ammonia and volatile organic compound emissions from poultry manure, Open Chem., 13 (2015) 967–973.
[27] K.V. Stepova, D.J. Maquarrie, I.M. Krip, Modified bentonites as adsorbents of hydrogen sulfide gases, Appl. Clay Sci., 42 (2009) 625–628.
[28] D. Nguyen-Thanh, K. Block, T.J. Bandosz, Adsorption of hydrogen sulfide on montmorillonites modified with iron, Chemosphere, 59 (2005) 343–353.
[29] F. Bernini, E. Castellini, D. Malferrari, G.R. Castro, C.I. Sainz Díaz, M.F. Brigatti, M. Borsari, Effective and selective trapping of volatile organic sulfur derivatives by montmorillonite intercalated with a μ-oxo Fe(III)-phenanthroline complex, ACS Appl. Mater. Interfaces, 9 (2017) 1045–1056.
[30] A.E.I. Elkhalifah, M. Azmi Bustam, A.M. Shariff, T. Murugesan, Selective adsorption of CO_2 on a regenerable amine-bentonite hybrid adsorbent, Appl. Clay Sci., 107 (2015) 213–219.
[31] B.E. Alver, Hydrogen adsorption on natural and sulphuric acid treated sepiolite and bentonite, Int. J. Hydrogen Energy, 43 (2018) 831–838.
[32] A. Gil, R. Trujillano, M.A. Vicente, S.A. Korili, Adsorption of nitrogen, hydrogen and carbon dioxide on alumina-pillared clays, Stud. Surf. Sci. Catal., 160 (2006) 327–334.
[33] M. Didier, L. Leone, J.-M. Greneche, E. Giffaut, L. Charlet, Adsorption of hydrogen gas and redox processes in clays, Environ. Sci. Technol., 46 (2012) 3574–3579.
[34] M. Li, L. Wang, J. Chen, Y. Jiang, W. Wang, Adsorption performance and mechanism of bentonite modified by ammonium bromide for gas-phase elemental mercury removal, J. Fuel Chem. Technol., 42 (2014) 1266–1272.
[35] S. Kwon, R.D. Vidic, Evaluation of two sulfur impregnation methods on activated carbon and bentonite for the production of elemental mercury sorbents, Environ. Eng. Sci., 17 (2000) 303–313.
[36] J. Jurng, T.G. Lee, G.W. Lee, S.J. Lee, B.H. Kim, J. Seier, Mercury removal from incineration flue gas by organic and inorganic adsorbents, Chemosphere, 47 (2002) 907–913.
[37] M.A. Stylianou, V.J. Inglezakis, K.G. Moustakas, S.P. Malamis, M.D. Loizidou, Removal of Cu(II) in fixed bed and batch reactors using natural zeolite and exfoliated vermiculite as adsorbents, Desalination, 215 (2007) 133–142.
[38] M.G. da Fonseca, M.M. de Oliveira, L.N.H. Arakaki, J.G.P. Espinola, C. Airoldi, Natural vermiculite as an exchanger support for heavy cations in aqueous solution, J. Colloid Interface Sci., 285 (2005) 50–55.
[39] M. Malandrino, O. Abollino, A. Giacomino, M. Aceto, E. Mentasti, Adsorption of heavy metals on vermiculite: influence of pH and organic ligands, J. Colloid Interface Sci., 299 (2006) 537–546.
[40] E. Álvarez-Ayuso, A. García-Sánchez, Removal of heavy metals from waste waters by vermiculites, Environ. Technol., 24 (2003) 615–625.
[41] N.A. Badawy, A.A. El-Bayaa, E. Abd AlKhalik, Vermiculite as an exchanger for copper(II) and Cr(III) ions, kinetic studies, Ionics, 16 (2010) 733–739.
[42] M.G. da Fonseca, M.M. de Oliveira, L.N.H. Arakaki, Removal of cadmium, zinc, manganese and chromium cations from aqueous solution by a clay mineral, J. Hazard. Mater., 137 (2006) 288–292.
[43] A.A. El-Bayaa, N.A. Badawy, E.A. AlKhalik, Effect of ionic strength on the adsorption of copper and chromium ions by vermiculite pure clay mineral, J. Hazard. Mater., 170 (2009) 1204–1209.
[44] G. Xueyi, K. Inoue, Elution of copper from vermiculite with environmentally benign reagents, Hydrometallurgy, 70 (2003) 9–21.
[45] M.R. Panuccio, A. Sorgonà, M. Rizzo, G. Cacco, Cadmium adsorption on vermiculite, zeolite and pumice: batch experimental studies, J. Environ. Manage., 90 (2009) 364–374.
[46] A. Sari, M. Tuzen, Removal of Cr(VI) from aqueous solution by Turkish vermiculite: equilibrium, thermodynamic and kinetic studies, Sep. Sci. Technol., 43 (2008) 3563–3581.
[47] A. Sarı, M. Tüzen, Adsorption of silver from aqueous solution onto raw vermiculite and manganese oxide-modified vermiculite, Microporous Mesoporous Mater., 170 (2013) 155–163.
[48] S. Hikmet, U. Turan, Removal of heavy metal ions from aqueous medium using Kuluncak (Malatya) vermiculites and effect of precipitation on removal, Appl. Clay Sci., 95 (2014) 1–8.
[49] K. Sumathi, Use of low-cost biological wastes and vermiculite for removal of chromium from tannery effluent, Bioresour. Technol., 96 (2005) 309–316.
[50] N.G. Turan, O. Ozgonenel, Optimizing copper ions removal from industrial leachate by explored vermiculite—a comparative analysis, J. Taiwan Inst. Chem. Eng., 44 (2013) 895–903.
[51] H. Long, P. Wu, L. Yang, Z. Huang, N. Zhu, Z. Hu, Efficient removal of cesium from aqueous solution with vermiculite of enhanced adsorption property through surface modification by ethylamine, J. Colloid Interface Sci., 428 (2014) 295–301.
[52] A.D. Purceno, A.P.C. Teixeira, A.B. Souza, J.D. Ardisson, J.P. de Mesquita, R.M. Lago, Ground vermiculite as catalyst for the Fenton reaction, Appl. Clay Sci., 69 (2012) 87–92.
[53] Z.-D. Wen, D.-W. Gao, Z. Li, N.-Q. Ren, Effects of humic acid on phthalate adsorption to vermiculite, Chem. Eng. J., 223 (2013) 298–303.
[54] N.G. Turan, A. Akdemir, O.N. Ergun, Removal of volatile organic compounds by natural materials during composting of poultry litter, Bioresour. Technol., 100 (2009) 798–803.
[55] A. Lu, D. Zhao, J. Li, C. Wang, S. Qin, Application of vermiculite and limestone to desulphurization and to the removal of dust during briquette combustion, Mineral. Mag., 67 (2003) 1243–1251.
[56] V. Inglezakis, Equilibrium and kinetic ion exchange studies of Pb^{2+}, Cr^{3+}, Fe^{3+} and Cu^{2+} on natural clinoptilolite, Water Res., 36 (2002) 2784–2792.
[57] V.J. Inglezakis, H.P. Grigoropoulou, Modeling of ion exchange of Pb^{2+} in fixed beds of clinoptilolite, Microporous Mesoporous Mater., 61 (2003) 273–282.
[58] V.J. Inglezakis, M.M. Loizidou, H.P. Grigoropoulou, Ion exchange studies on natural and modified zeolites and the concept of exchange site accessibility, J. Colloid Interface Sci., 275 (2004) 570–576.

[59] V.J. Inglezakis, M.A. Stylianou, D. Gkantzou, M.D. Loizidou, Removal of Pb(II) from aqueous solutions by using clinoptilolite and bentonite as adsorbents, Desalination, 210 (2007) 248–256.
[60] M.A. Stylianou, M.P. Hadjiconstantinou, V.J. Inglezakis, K.G. Moustakas, M.D. Loizidou, Use of natural clinoptilolite for the removal of lead, copper and zinc in fixed bed column, J. Hazard. Mater., 143 (2007) 575–581.
[61] M.A. Stylianou, V.J. Inglezakis, M. Loizidou, Comparison of Mn, Zn, and Cr removal in fluidized- and fixed-bed reactors by using clinoptilolite, Desal. Wat. Treat., 53 (2015) 3355–3362.
[62] M.A.S.D. de Barros, N.R.C.F. Machado, F.V. Alves, E.F. Sousa-Aguiar, Ion exchange mechanism of Cr^{3+} on naturally occurring clinoptilolite, Braz. J. Chem. Eng., 14 (1997) 233–241.
[63] N. Bektaş, S. Kara, Removal of lead from aqueous solutions by natural clinoptilolite: equilibrium and kinetic studies, Sep. Purif. Technol., 39 (2004) 189–200.
[64] L. Ćurković, Š. Cerjan-Stefanović, T. Filipan, Metal ion exchange by natural and modified zeolites, Water Res., 31 (1997) 1379–1382.
[65] M. Doula, A. Ioannou, A. Dimirkou, Copper adsorption and Si, Al, Ca, Mg, and Na release from clinoptilolite, J. Colloid Interface Sci., 245 (2002) 237–250.
[66] E. Erdem, N. Karapinar, R. Donat, The removal of heavy metal cations by natural zeolites, J. Colloid Interface Sci., 280 (2004) 309–314.
[67] A. Langella, M. Pansini, P. Cappelletti, B. de Gennaro, M. de' Gennaro, C. Colella, NH_4^+, Cu^{2+}, Zn^{2+}, Cd^{2+} and Pb^{2+} exchange for Na^+ in a sedimentary clinoptilolite, North Sardinia, Italy, Microporous Mesoporous Mater., 37 (2000) 337–343.
[68] M. Loizidou, K.J. Haralambous, A. Loukatos, D. Dimitrakopoulou, Natural zeolites and their ion exchange behavior towards chromium, J. Environ. Sci. Health, Part A, 27 (1992) 1759–1769.
[69] E. Maliou, M. Loizidou, E. Spyrellis, Uptake of lead and cadmium by clinoptilolite, Sci. Total Environ., 149 (1994) 139–144.
[70] E. Maliou, M. Malamis, P.O. Sakellarides, Lead and cadmium removal by ion exchange, Water Sci. Technol., 25 (1992) 133–138.
[71] M.V. Mier, R.L. Callejas, R. Gehr, B.E.J. Cisneros, P.J.J. Alvarez, Heavy metal removal with Mexican clinoptilolite, Water Res., 35 (2001) 373–378.
[72] N. Medvidovic, J. Peric, M. Trgo, Column performance in lead removal from aqueous solutions by fixed bed of natural zeolite–clinoptilolite, Sep. Purif. Technol., 49 (2006) 237–244.
[73] A.H. Oren, A. Kaya, Factors affecting adsorption characteristics of Zn^{2+} on two natural zeolites, J. Hazard. Mater., 131 (2006) 59–65.
[74] P. Papachristou, K.J. Haralambous, M. Loizidou, N. Spyrellis, Studies on the nickel removal from aqueous solutions, J. Environ. Sci. Health, Part A, 28 (1993) 135–142.
[75] J. Perić, M. Trgo, N. Vukojević Medvidović, Removal of zinc, copper and lead by natural zeolite—a comparison of adsorption isotherms, Water Res., 38 (2004) 1893–1899.
[76] R. Petrus, J.K. Warchoł, Heavy metal removal by clinoptilolite. An equilibrium study in multi-component systems, Water Res., 39 (2005) 819–830.
[77] A. Top, S. Ülkü, Silver, zinc, and copper exchange in a Na-clinoptilolite and resulting effect on antibacterial activity, Appl. Clay Sci., 27 (2004) 13–19.
[78] M. Turan, U. Mart, B. Yuksel, M. Celik, Lead removal in fixed-bed columns by zeolite and sepiolite, Chemosphere, 60 (2005) 1487–1492.
[79] M.S. Celik, B. Ozdemir, M. Turan, I. Koyuncu, G. Atesok, H.Z. Sarikaya, Removal of ammonia by natural clay minerals using fixed and fluidised bed column reactors, Water Sci. Technol. Water Supply, 1 (2001) 81–88.
[80] A.A. Zorpas, V.J. Inglezakis, M. Stylianou, V. Irene, Sustainable treatment method of a high concentrated NH_3 wastewater by using natural zeolite in closed-loop fixed bed systems, Open Environ. Sci., 4 (2009) 1–7.
[81] A. Cincotti, N. Lai, R. Orrù, G. Cao, Sardinian natural clinoptilolites for heavy metals and ammonium removal: experimental and modeling, Chem. Eng. J., 84 (2001) 275–282.
[82] P. Jun-Boum, S.-H. Lee, J.-W. Lee, C.-Y. Lee, Lab scale experiments for permeable reactive barriers against contaminated groundwater with ammonium and heavy metals using clinoptilolite (01-29B), J. Hazard. Mater., 95 (2002) 65–79.
[83] A. Papadopoulos, E.G. Kapetanios, M. Loizidou, Studies on the use of clinoptilolite for ammonia removal from leachates, J. Environ. Sci. Health, Part A, 31 (1996) 211–220.
[84] M. Sarioglu, Removal of ammonium from municipal wastewater using natural Turkish (Dogantepe) zeolite, Sep. Purif. Technol., 41 (2005) 1–11.
[85] U. Wingenfelder, C. Hansen, G. Furrer, R. Schulin, Removal of heavy metals from mine waters by natural zeolites, Environ. Sci. Technol., 39 (2005) 4606–4613.
[86] M. Tomasevic-Canovic, V.M.A. Dakovic, D. Stojsic, The effect of exchangeable cations in clinoptilolite and montmorillonite on the adsorption of aflatoxin B1, J. Serb. Chem. Soc., 66 (2001) 555–561.
[87] A.E. Papadopoulos, M.A. Stylianou, C.P. Michalopoulos, K.G. Moustakas, K.M. Hapeshis, E.E.I. Vogiatzidaki, M.D. Loizidou, Performance of a new household composter during in-home testing, Waste Manage. (Oxford), 29 (2009) 204–213.
[88] M.A. Stylianou, V.J. Inglezakis, K.G. Moustakas, M.D. Loizidou, Improvement of the quality of sewage sludge compost by adding natural clinoptilolite, Desalination, 224 (2008) 240–249.
[89] E. Álvarez-Ayuso, Purification of metal electroplating waste waters using zeolites, Water Res., 37 (2003) 4855–4862.
[90] P. Bosi, D. Creston, L. Casini, Production performance of dairy cows after the dietary addition of clinoptilolite, Ital. J. Anim. Sci., 1 (2010) 187.
[91] K. Deligiannis, T. Lainas, G. Arsenos, E. Papadopoulos, P. Fortomaris, D. Kufidis, C. Stamataris, D. Zygoyiannis, The effect of feeding clinoptilolite on food intake and performance of growing lambs infected or not with gastrointestinal nematodes, Livestock Prod. Sci., 96 (2005) 195–203.
[92] J.P. Goff, The monitoring, prevention, and treatment of milk fever and subclinical hypocalcemia in dairy cows, Vet. J., 176 (2008) 50–57.
[93] P.-D. Katsoulos, N. Roubies, N. Panousis, G. Arsenos, E. Christaki, H. Karatzias, Effects of long-term dietary supplementation with clinoptilolite on incidence of parturient paresis and serum concentrations of total calcium, phosphate, magnesium, potassium, and sodium in dairy cows, Am. J. Vet. Res., 66 (2005) 2081–2085.
[94] P.D. Katsoulos, N. Panousis, N. Roubies, E. Christaki, G. Arsenos, H. Karatzias, Effects of long-term feeding of a diet supplemented with clinoptilolite to dairy cows on the incidence of ketosis, milk yield and liver function, Vet. Rec., 159 (2006) 415–418.
[95] M.A. Norouzian, R. Valizadeh, A.A. Khadem, A. Afzalzadeh, A. Nabipour, The effects of feeding clinoptilolite on hematology, performance, and health of newborn lambs, Biol. Trace Elem. Res., 137 (2010) 168–176.
[96] T.R. Overton, M.R. Waldron, Nutritional management of transition dairy cows: strategies to optimize metabolic health, J. Dairy Sci., 87 (2004) E105–E119.
[97] D.S. Papaioannou, S.C. Kyriakis, A. Papasteriadis, N. Roumbies, A. Yannakopoulos, C. Alexopoulos, A field study on the effect of in-feed inclusion of a natural zeolite (clinoptilolite) on health status and performance of sows/gilts and their litters, Res. Vet. Sci., 72 (2002) 51–59.
[98] D. Papaioannou, P.D. Katsoulos, N. Panousis, H. Karatzias, The role of natural and synthetic zeolites as feed additives on the prevention and/or the treatment of certain farm animal diseases: a review, Microporous Mesoporous Mater., 84 (2005) 161–170.
[99] P.J. Rajala-Schultz, Y.T. Gröhn, C.E. McCulloch, Effects of milk fever, ketosis and lameness on milk yield in dairy cows, J. Dairy Sci., 82 (1999) 288–294.

[100] G. Rodríguez-Fuentes, M.A. Barrios, A. Iraizoz, I. Perdomo, B. Cedré, Enterex: anti-diarrheic drug based on purified natural clinoptilolite, Zeolites, 19 (1997) 441–448.
[101] G. Rodríguez-Fuentes, A.R. Denis, M.A. Barrios Álvarez, A.I. Colarte, Antacid drug based on purified natural clinoptilolite, Microporous Mesoporous Mater., 94 (2006) 200–207.
[102] A.A. Sadeghi, P. Shawrang, Effects of natural zeolite clinoptilolite on passive immunity and diarrhea in newborn Holstein calves, Livestock Sci., 113 (2008) 307–310.
[103] M. Bonferoni, G. Cerri, M. Degennaro, C. Juliano, C. Caramella, Zn^{2+}-exchanged clinoptilolite-rich rock as active carrier for antibiotics in anti-acne topical therapy: in-vitro characterization and preliminary formulation studies, Appl. Clay Sci., 36 (2007) 95–102.
[104] M.I. Carretero, M. Pozo, Clay and non-clay minerals in the pharmaceutical industry, Appl. Clay Sci., 46 (2009) 73–80.
[105] G. Cerri, M. Degennaro, M. Bonferoni, C. Caramella, Zeolites in biomedical application: Zn-exchanged clinoptilolite-rich rock as active carrier for antibiotics in topical therapy, Appl. Clay Sci., 27 (2004) 141–150.
[106] L. Cheng-Fang, L. Shun-Shin, L. Herng-Yuh, L. Yichin, Stabilization of cadmium contaminated soils using synthesized zeolite, J. Hazard. Mater., 60 (1998) 217–226.
[107] E.H. Rybicka, B. Jedrzejczyk, Preliminary studies on mobilisation of copper and lead from contaminated soils and readsorption on competing sorbents, Appl. Clay Sci., 10 (1995) 259–268.
[108] M.A. Stylianou, V.J. Inglezakis, M.D. Loizidou, Effects of Zeolite Addition on Soil Chemistry-Open Field Experiments, Protection and Restoration of the Environment VII, Myconos, Greece, 2004.
[109] H. Faghihian, M. Ghannadi Marageh, H. Kazemian, The use of clinoptilolite and its sodium form for removal of radioactive cesium, and strontium from nuclear wastewater and Pb^{2+}, Ni^{2+}, Cd^{2+}, Ba^{2+} from municipal wastewater, Appl. Radiat. Isot., 50 (1999) 655–660.
[110] E. Valcke, B. Engels, A. Cremers, The use of zeolites as amendments in radiocaesium- and radiostrontium-contaminated soils: a soil-chemical approach. Part I: Cs-K exchange in clinoptilolite and mordenite, Zeolites, 18 (1997) 205–211.
[111] E.G. Kapetanios, M. Loizidou, Heavy metal removal by zeolite in tomato cultivation using compost, Acta Hortic., 302 (1992) 63–74.
[112] A. Zorpas, Heavy metal uptake by natural zeolite and metals partitioning in sewage sludge compost, Bioresour. Technol., 72 (2000) 113–119.
[113] A.A. Zorpas, V. Inglezakis, M. Loizidou, H. Grigoropoulou, Particle size effects on uptake of heavy metals from sewage sludge compost using natural zeolite clinoptilolite, J. Colloid Interface Sci., 250 (2002) 1–4.
[114] P. Kosobucki, M. Kruk, B. Buszewski, Immobilization of selected heavy metals in sewage sludge by natural zeolites, Bioresour. Technol., 99 (2008) 5972–5976.
[115] D. Mück-Šeler, N. Pivac, The effect of natural clinoptilolite on the serotonergic receptors in the brain of mice with mammary carcinoma, Life Sci., 73 (2003) 2059–2069.
[116] F.A. Mupton, La roca magica: uses of natural zeolites in agriculture and industry, Proc. Natl. Acad. Sci. USA, 96 (1999) 3463–3470.
[117] K. Pavelic, M. Hadzija, K. Auerbach, P. Carraro, Medical Applications of Zeolite, S. Auerbach, K. Carraro, P.D.M. Dekker, Eds., Handbook of Zeolite Science and Technology, 2003, pp. 1141.
[118] K. Pavelic, M. Katic, V. Sverko, T. Marotti, B. Bosnjak, T. Balog, R. Stojkovic, M. Radacic, M. Colic, M. Poljak-Blazi, Immunostimulatory effect of natural clinoptilolite as a possible mechanism of its antimetastatic ability, J. Cancer Res. Clin. Oncol., 128 (2002) 37–44.
[119] K. Pavelic, M. Hadžija, L. Bedrica, J. Pavelić, I. Đikić, M. Katić, M. Kralj, M.H. Bosnar, S. Kapitanović, M. Poljak-Blaži, Š. Križanac, R. Stojković, M. Jurin, B. Subotić, M. Čolić, Natural zeolite clinoptilolite: new adjuvant in anticancer therapy, J. Mol. Med., 78 (2001) 708–720.
[120] N. Zarkovic, K. Zarkovic, M. Kralj, S. Borovic, S. Sabolovic, M.P. Blazi, A. Cipak, K. Pavelic, Anticancer and antioxidative effects of micronized zeolite clinoptilolite, Anticancer Res., 23 (2003) 1589–1595.
[121] H.W. Pickering, N.W. Menzies, M.N. Hunter, Zeolite/rock phosphate—a novel slow release phosphorus fertiliser for potted plant production, Sci. Hortic., 94 (2002) 333–343.
[122] M. Ozekmekci, G. Salkic, M.F. Fellah, Use of zeolites for the removal of H_2S: a mini-review, Fuel Process. Technol., 139 (2015) 49–60.
[123] I.M. Morris, W. Midlands, S. Charles, F. Robinson, B. Soar, D. Frederick, Adsorbents for Separating Nitrogen from a Feed Gas, No. 5993516, BG PLC, Berkshire, USA, 1999.
[124] C.C. Chao, H. Rastelli, Process for Preparing Zeolitic Adsorbents, No. 5045515, UOP, Des Plaines, USA, 1991.
[125] C.C. Chao, H. Rastelli, Process for Modifying Clinoptilolite Adsorbent, No. 5116793, UOP, Des Plaines, USA, 1992.
[126] C.C. Chao, H. Rastelli, Process for Purification of Hydrocarbons Using Metal Exchanged Clinoptilolite to Remove Carbon Dioxide, 4935580, UOP, Des Plaines, USA, 1990.
[127] M.W. Ackley, S.U. Rege, H. Saxena, Application of natural zeolites in the purification and separation of gases, Microporous Mesoporous Mater., 61 (2003) 25–42.
[128] G. Narin, S. Ülkü, Adsorption of NO in clinoptilolite-rich zeolitic mineral by concentration pulse chromatography method, Microporous Mesoporous Mater., 234 (2016) 120–129.
[129] O. Korkuna, R. Leboda, J. Skubiszewska-Zieba, T. Vrublevska, V.M. Gunko, J. Ryczkowski, Structural and physicochemical properties of natural zeolites: clinoptilolite and mordenite, Microporous Mesoporous Mater., 87 (2006) 243–254.
[130] F. Crejtak, I. Horvath, M. Kubranova, J. Krajcovoc, The acidity of dealuminated clinoptilolite investigated by DSC, DTA and TG methods, Thermochim. Acta, 207 (1992) 209–217.
[131] M. Foldesova, P. Lukac, P. Dillinger, V. Balek, S. Svetik, Thermochemical properties of chemically modified zeolite, J. Therm. Anal. Calorim., 58 (1999) 671–675.
[132] B. Erdogan, M. Sakızcı, E. Yorukogulları, Characterization and ethylene adsorption of natural and modified clinoptilolites, Appl. Surf. Sci., 254 (2008) 2450–2457.
[133] T. Perraki, A. Orfanoudaki, Mineralogical study of zeolites from Pentalofos area, Thrace, Greece, Appl. Clay Sci., 25 (2004) 9–16.
[134] A.D. Vujakovic, M.A. Djuricic, M.R. Tomasevic-Canovic, Thermal study of surfactant and anion adsorption on clinoptilolite, J. Therm. Anal. Calorim., 63 (2001) 161–172.
[135] M.K. Doula, Synthesis of a clinoptilolite–Fe system with high Cu sorption capacity, Chemosphere, 67 (2007) 731–740.
[136] P. Castaldi, L. Santona, C. Cozza, V. Giuliano, C. Abbruzzese, V. Nastro, P. Melis, Thermal and spectroscopic studies of zeolites exchanged with metal cations, J. Mol. Struct., 734 (2005) 99–105.
[137] B. Tomazovic, T. Ceranic, G. Sijaric, The properties of the NH_4-clinoptilolite. Part 1, Zeolites, 16 (1996) 301–308.
[138] M. Rehakova, A. Sopkova, V. Sepelak, J. Briancin, T. Wadsten, Natural zeolitic material of the clinoptilolite type and its AgI form, J. Inclusion Phenom. Mol. Recognit. Chem., 23 (1995) 157–163.
[139] F.E. Trigueiro, D.F.J. Monteiro, F.M.Z. Zotin, E.F. Sousa-Aguiar, Thermal stability of Y zeolites containing different rare earth cations, J. Alloys Compd., 344 (2002) 337–341.
[140] Y. Sarikaya, M. Onal, B. Baran, T. Alemdaroglu, The effect of thermal treatment on some of the physicochemical properties of a bentonite, Clays Clay Miner., 48 (2000) 557–562.
[141] A. Tabak, B. Afsin, B. Caglar, E. Koksal, Characterization and pillaring of a Turkish bentonite (Resadiye), J. Colloid Interface Sci., 313 (2007) 5–11.
[142] J. Li, L. Zhu, W. Cai, Characteristics of organobentonite prepared by microwave as a sorbent to organic contaminants in water, Colloids Surf., A, 281 (2006) 177–183.
[143] B. Caglar, B. Afsin, A. Tabak, E. Eren, Characterization of the cation-exchanged bentonites by XRPD, ATR, DTA/TG analyses and BET measurement, Chem. Eng. J., 149 (2009) 242–248.

[144] A. Tabak, B. Afsin, S.F. Aygun, H. Icbudak, Phenanthroline Cu(II)-bentonite composite characterization, J. Therm. Anal. Calorim., 81 (2005) 311–314.
[145] M. Onal, Y. Sarikaya, Thermal behavior of a bentonite, J. Therm. Anal. Calorim., 90 (2007) 167–172.
[146] A. Justo, J.L. Perez-Rodríguez, P.J. Sanchez-Soto, Thermal study of vermiculites and mica-vermiculite interstratifications, J. Therm. Anal., 40 (1993) 59–65.
[147] L.A. Perez-Maqueda, V. Balek, J. Poyato, J.L. Perez-Rodriquez, J. Subrt, I.M. Bountsewa, I.N. Beckman, Z. Malek, Study of natural and ion exchanged vermiculite by emanation thermal analysis, TG, DTA and XRD, J. Therm. Anal. Calorim., 71 (2003) 715–726.
[148] R.L. Kerns, C.J. Mankin, Compositional variation of a vermiculite as related to particle size, Clays Clay Miner., 15 (1967) 163–177.
[149] A. Ruiz-Conde, A. Ruizamil, J.L. Perez-Rodriguez, P.J. Sanchez-Soto, F.A.d.l. Cruz, Interaction of vermiculite with aliphatic amides (formamide, acetamide and propoinamide): formation and study of interstratified phases in the transformation of Mg- to NH_4-vermiculite, Clays Clay Miner., 45 (1997) 311–326.
[150] M. Uehara, A. Yamzaki, T. Umezawa, K. Takahashi, S. Tsutsumi, A nickel hydroxide-vermiculite complex; preparation and characterization, Clays Clay Miner., 47 (1999) 726–731.
[151] M.C.J.D. Haro, J.M.M. Blanes, J. Poyato, L.A. Perez-Maqueda, A. Lerf, J.L.P. Rodríguez, Effects of mechanical treatment and exchanged cation on the microporosity of vermiculite, J. Phys. Chem. Solids, 65 (2004) 435–439.
[152] M.C.J.D. Haro, M.L.A. Perez, E.T. Stepkowska, J.M. Martínez, J.L. Perez-Rodriguez, The influence of exchangeable cation on thermal behaviour of ground vermiculite, J. Therm. Anal. Calorim., 71 (2003) 761–771.
[153] V.J. Inglezakis, The concept of "capacity" in zeolite ion-exchange systems, J. Colloid Interface Sci., 281 (2005) 68–79.
[154] V.J. Inglezakis, S.G. Poulopoulos, Adsorption, Ion Exchange and Catalysis: Design of Operations and Environmental Applications, Elsevier, Netherlands, 2006.
[155] S. Brunauer, P.H. Emmett, E. Teller, Adsorption of gases in multimolecular layers, J. Am. Chem. Soc., 60 (1938) 309–319.
[156] M.D. Ruthven, Principles of Adsorption and Adsorption Process, Wiley & Sons, New York, 1984.
[157] W. Mozgawa, M. Sitarz, M. Rokita, Spectroscopic studies of different aluminosilicate structures, J. Mol. Struct., 511–512 (1999) 251–257.
[158] G.E. Christidis, D. Moraetis, E. Keheyan, L. Akhalbedashvili, N. Kekelidze, R. Gevorkyan, H. Yeritsyan, H. Sargsyan, Chemical and thermal modification of natural HEU-type zeolitic materials from Armenia, Georgia and Greece, Appl. Clay Sci., 24 (2003) 79–91.
[159] M.S. Joshi, V.V. Joshi, A.L. Choudhari, M.W. Kasture, Structural studies of natural heulandite using infrared spectroscopy, Mater. Chem. Phys., 48 (1997) 160–163.
[160] K. Elaiopoulos, T. Perraki, E. Grigoropoulou, Mineralogical study and porosimetry measurements of zeolites from Scaloma area, Thrace, Greece, Microporous Mesoporous Mater., 112 (2008) 441–449.
[161] M. Majdan, M. Kowalska-Ternesa, S. Pikusa, P. Staszczuka, H. Skrzypekb, E. Zie, Vibrational and scanning electron microscopy study of the mordenite modified by Mn, Co, Ni, Cu, Zn and Cd, J. Mol. Struct., 649 (2003) 279–285.
[162] W. Mozgawa, The influence of some heavy metals cations on the FTIR spectra of zeolites, J. Mol. Struct., 555 (2000) 299–304.
[163] T. Perraki, G. Kakali, F. Kontoleon, The effect of natural zeolites on the early hydration of Portland cement, Microporous Mesoporous Mater., 61 (2003) 205–212.
[164] T. Perraki, A. Orfanoudaki, Mineralogical composition and physical properties of bentonites of the island of Milos, Min. Wealth, 104 (1997) 35–42.
[165] R.E. Grim, Clay Mineralogy, McGraw-Hill, New York, 1953.
[166] P.S. Nayak, B.K. Singh, Instrumental characterization of clay by XRF, XRD and FTIR, Bull. Mater. Sci., 30 (2007) 235–238.
[167] K. Bukka, J.D. Miller, FTIR study of deuterated montmorillonites: structural features relevant to pillared clay stability, Clays Clay Miner., 40 (1992) 92–102.
[168] N.G. White, J.B. Dixon, Soil Mineralogy Laboratory Manual Agronomy 626, 11th ed., Soil & Crop Sciences Department, Texas A & M University, 2003.
[169] O. Gok, A. Ozcan, B. Erdem, A.S. Ozcan, Prediction of the kinetics, equilibrium and thermodynamic parameters of adsorption of copper(II) ions onto 8-hydroxy quinoline immobilized bentonite, Colloids Surf., A, 317 (2008) 174–185.
[170] J. Zhang, A. Wang, Study on superabsorbent composites. IX: synthesis, characterization and swelling behaviors of polyacrylamide/clay composites based on various clays, React. Funct. Polym., 67 (2007) 737–745.
[171] N. Venkatathri, Characterization and catalytic properties of a naturally occurring clay, Bentonite, Bull. Catal. Soc. India, 5 (2006) 61–72.
[172] D. Righi, S. Petit, A. Bouchet, Characterization of hydroxy-interlayered vermiculite and illite/smectite interstratified minerals from the weathering of chlorite in a cryorthod, Clays Clay Miner., 41 (1993) 484–495.
[173] P.M. Schosseler, A.U. Gehring, Transition metals in llano vermiculite samples: an EPR study, Clays Clay Miner., 44 (1996) 470–478.
[174] G.V. Tsitsishvili, T.G. Andronikashvili, G.N. Kirov, L.D. Filizova, Natural Zeolites, Chichester, UK, 1992.
[175] S. Wang, Y. Peng, Natural zeolites as effective adsorbents in water and wastewater treatment, Chem. Eng. J., 156 (2010) 11–24.
[176] K. Athanasiadis, B. Helmreich, Influence of chemical conditioning on the ion exchange capacity and on kinetic of zinc uptake by clinoptilolite, Water Res., 39 (2005) 1527–1532.
[177] A. Mellah, S. Chegrouche, The removal of zinc from aqueous solutions by natural bentonite, Water Res., 31 (1997) 621–629.
[178] T. Perraki, Industrial Minerals and Rocks (Notes), NTUA, School of Mining and Metallurgical Engineering, Department of Geological Sciences, Athens, 2007, pp. 117–130.
[179] N. Kantiranis, A. Filippidis, A. Drakoulis, A. Tsirampidis, Study of Binding Capacity of Milos Bentonite and Attapulgite of Grevena, Second Conference of the Economic Geology, Mineralogy and Geochemistry, Thessaloniki, 2005, pp. 105–112.
[180] S.A. Khan, R. Rehman, M.A. Khan, Adsorption of chromium (III), chromium (IV) and silver (I) on bentonite, Waste Manage. (Oxford), 15 (1995) 271–282.
[181] G. Bereket, A.Z. Arog, M.Z. Özel, Removal of Pb(II), Cd(II), Cu(II), and Zn(II) from aqueous solutions by adsorption on bentonite, J. Colloid Interface Sci., 187 (1997) 338–343.
[182] A. Bourliva, K. Michailidis, C. Sikalidis, G. Trontsios, Removal of lead (Pb^{2+}) and zinc (Zn^{2+}) from aqueous solutions by adsorption on vermiculite from Ascos area in Macedonia (Northern Greece), Bull. Geol. Soc. Greece, 36 (2004) 182–191.
[183] N.C. Das, M. Bandyopadhyay, Removal of lead by vermiculite medium, Appl. Clay Sci., 6 (1991) 221–231.
[184] F. Mumpton, Clinoptilolite redefined, Am. Mineral., 45 (1960) 351–369.
[185] M.S. Doula, Adsorption of Heavy Metals from Inorganic Colloids (Zeolites), National Technical University of Athens, Athens, Greece, 2003.
[186] E.D. Malliou, Removal of Heavy Metal Ions from Aqueous Solution, Using Greek Natural Zeolites, National Technical University of Athens, Athens, Greece, 1994.
[187] D.P. Dobocan C.A., E. Culea, V. Topa, Analysis of the Zeolite Volcanic Tuffs from Cluz County, Romania, Proc. 13th International Conference of Environmental Science and Technology Athens, Greece, 5–7 September 2013.
[188] K. Elaiopoulos, T. Perraki, E. Grigoropoulou, Monitoring the effect of hydrothermal treatments on the structure of a natural zeolite though a combined XRD, FTIR, XRF, SEM and N_2-porosimetry analysis, Microporous Mesoporous Mater., 134 (2010) 29–43.
[189] L. Zhirong, M. Azhar Uddin, S. Zhanxue, FT-IR and XRD analysis of natural Na-bentonite and Cu(II)-loaded Na-bentonite, Spectrochim. Acta, Part A, 79 (2011) 1013–1016.

[190] M.F. Brigatti, S. Colonna, D. Malferrari, L. Medici, L. Poppi, Mercury adsorption by montmorillonite and vermiculite: a combined XRD, TG-MS, and EXAFS study, Appl. Clay Sci., 28 (2005) 1–8.
[191] I.K. Ilia, M.G. Stamatakis, T.S. Perraki, Mineralogy and technical properties of clayey diatomites from north and central Greece, Cent. Eur. J. Geosci., 1 (2009) 393–403.
[192] V.P. Moreno, J.J.C. Arellano, H.B. Ramırez, Characterization and preparation of porous membranes with a natural Mexican zeolite, J. Phys.: Condens. Matter, 16 (2004) S2345–S2352.
[193] M. Albayrak, A. Yorukoglu, S. Karahan, S. Atlihan, H.Y. Aruntas, I. Girgin, Influence of zeolite additive on properties of autoclaved aerated concrete, Build. Environ., 42 (2007) 3161–3165.
[194] A. Gil, P. Grange, Application of the Dubinin-Radushkevich and Dubinin-Astakhov equations in the characterization of microporous solids, Colloids Surf., A, 113 (1996) 39–50.
[195] M. Suzuki, Adsorption Engineering, Kodansha, Tokyo, 1990.
[196] V.J. Inglezakis, Solubility-normalized Dubinin–Astakhov adsorption isotherm for ion-exchange systems, Microporous Mesoporous Mater., 103 (2007) 72–81.